

OLD DOMINION UNIVERSITY RESEARCH FOUNDATION

DEPARTMENT OF CHEMICAL SCIENCES
SCHOOL OF SCIENCES AND HEALTH PROFESSIONS
OLD DOMINION UNIVERSITY
NORFOLK, VIRGINIA 23508

COMPUTATIONAL SOLUTION OF
ATMOSPHERIC CHEMISTRY PROBLEMS

By

Jawed Jafri, Co-Principal Investigator

Robert L. Ake, Principal Investigator

Final Report

For the period ended December 31, 1985

Prepared for the
National Aeronautics and Space Administration
Langley Research Center
Hampton, VA 23665

Under

Research Grant NSG-1393

Dr. Donald H. Phillips, Technical Monitor

IRD-Materials Characterization Instrumentation Section

August 1986

N87-11353

(NASA-CR-179803) COMPUTATIONAL SOLUTION OF
ATMOSPHERIC CHEMISTRY PROBLEMS Final
Report, period ending 31 Dec. 1985 (Old
Dominion Univ.) 80 p CSDL 13B

G3/45
Unclas
43767

DEPARTMENT OF CHEMICAL SCIENCES
SCHOOL OF SCIENCES AND HEALTH PROFESSIONS
OLD DOMINION UNIVERSITY
NORFOLK, VIRGINIA 23508

COMPUTATIONAL SOLUTION OF
ATMOSPHERIC CHEMISTRY PROBLEMS

By

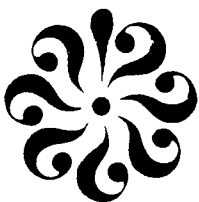
Jawed Jafri, Co-Principal Investigator

Robert L. Ake, Principal Investigator

Final Report
For the period ended December 31, 1985

Prepared for the
National Aeronautics and Space Administration
Langley Research Center
Hampton, VA 23665

Under
Research Grant NSG-1393
Dr. Donald H. Phillips, Technical Monitor
IRD-Materials Characterization Instrumentation Section



Submitted by the
Old Dominion University Research Foundation
P. O. Box 6369
Norfolk, Virginia 23508

August 1986

TABLE OF CONTENTS

	<u>Page</u>
INTRODUCTION.....	1
I. THEORETICAL STUDIES OF GROUND AND LOW-LYING EXCITED STATES OF ClO_2	1
II. GROUND AND EXCITED STATE POTENTIAL ENERGY SURFACES OF THE METHYL PEROXY RADICAL, CH_3O_2	3
III. ELECTRONIC STATES OF THE FO RADICAL.....	17
IV. THEORETICAL STUDIES OF $\text{SO}_2 \cdot (\text{H}_2\text{O})_n$ COMPLEXES.....	37
ADDENDUM.....	53
ACKNOWLEDGMENTS.....	54
REFERENCES.....	55
APPENDIX.....	57

LIST OF TABLES

<u>Table</u>	<u>Page</u>
1 Energies of the lowest $^2A''$ and $^2A'$ states of CH_3O_2 as a function of $R(\text{O}-\text{O})$; $R(\text{C}-\text{O})$ fixed at 2.725 bohr.....	7
2 Energies of the lowest $^2A''$ and $^2A'$ states of CH_3O_2 as a function of $R(\text{C}-\text{O})$; $R(\text{O}-\text{O})$ fixed at 2.783 bohr.....	8
3 Energies of the first two $^2A''$ states along the $R(\text{O}-\text{O})$ stretching coordinate with $R(\text{C}-\text{O}) = 2.7483$ bohr.....	9
4 Energies (in Hartrees), for the first two $^2A''$ states in the $R(\text{C}-\text{O})$ stretching coordinate. $R(\text{O}-\text{O})$ was fixed at 2.5606 bohr.....	10
5 Energies (in Hartrees) of the X^2A'' and $2^2A''$ states along the stretching coordinate along a 45° angle through the plane defined by $R(\text{C}-\text{O})$ and $R(\text{O}-\text{O})$ stretches. The first and second root $^2A''$ states employed approximate natural orbitals determined separately.....	11
6 Nature of Ground State Wave function for FO at Various Levels of Computation.....	21
7 FO Ground State Energies (Hartrees) as a Function of Internuclear Separation at Various Levels of Computation.....	22
8 Energies (Hartrees) for the 2π Ground and Excited States of FO at MCSCF Level.....	23

TABLE OF CONTENTS - continued

LIST OF TABLES - continued

<u>Table</u>	<u>Page</u>
9 Coefficients of Important CSF's for $2^2\pi$ and $3^2\pi$ States of FO as a Function of Internuclear Separation....	24
10 First Order CI Energies (Hartrees) for π Excited States of FO.....	25
11 Full Valence Excited State Wave Functions of FO.....	26
12 MCSCF Energies (Hartrees) for $^4\Sigma^-$, $^2\Sigma^-$, $^2\Sigma^+$, and $^2\Delta$ Excited States of FO.....	27
13 Expectation Values of the Dipole Moment of FO.....	28
14 Dipole Moments of $X^2\pi$ and the $^2\pi$ States of FO at Full Valance CI Level.....	29
15 SD-CI Vibrational Frequencies and Transitions Moments	30
16 Transition Moments of FO at Full Valance Level of Computation at 2.60 Bohr Internuclear Separation.....	31
17 Total energies (Hartrees) and binding energies (milliHartrees in parentheses) of conformations I and II and the separated fragments showing the effects of configuration interaction..	46
18 Mulliken population analysis of conformations I and II and separated fragments showing effect of configuration interaction.....	47
19 SCF total energies (Hartrees) and binding energies (milli-Hartrees in parentheses) of $SO_2 \cdot (H_2O)_n$ complexes.....	48
20 Dipole moments (in Debyes) for fragments and selected complexes from SCF geometry optimizations.....	49

LIST OF FIGURES

<u>Figure</u>	<u>Page</u>
1 Potential energy of the lowest $^2A''$ and $^2A'$ states of CH_3O_2 along the R(O-O) coordinate. The calculations used a double zeta basis and selected "pseudo first order" CI. R(C-O) fixed at 2.725 bohr.....	12
2 Potential energy of the lowest $^2A''$ and $^2A'$ states of the CH_3O_2 radical along the R(C-O) coordinate. The calculations used a double zeta basis and selected "pseudo first order" CI. R(O-O) fixed at 2.783 bohr.....	13

TABLE OF CONTENTS - concluded

LIST OF FIGURES - concluded

<u>Figure</u>		<u>Page</u>
3	Potential energy of the X^2A'' and $2^2A''$ states of CH_3O_2 along the $R(O-O)$ coordinate. The calculations used a double zeta basis augmented by polarization functions and a selected single and double CI in approximate natural orbital basis. $R(C-O)$ fixed at 2.7483 bohr.....	14
4	Potential energy of the X^2A'' and $2^2A''$ states of CH_3O_2 along the $R(C-O)$ coordinate. The calculations used a double zeta basis augmented by polarization functions and selected "single and double" CI in approximate natural orbital basis. $R(O-O)$ fixed at 2.5606 bohr.....	15
5	Potential energy of X^2A'' and $2^2A''$ CH_3O_2 along 45° angle in the plane defined by $R(C-O)$ and $R(O-O)$ coordinates. The calculations used a double zeta basis augmented by polarization functions and selected singles and doubles CI in approximate natural orbital basis.....	16
6	Potential Energy curves for the $X^2\pi$ State of FO	32
7	Full Valence MCSCF Potential Energy Curves for Ground and Excited 2π States of FO.....	33
8	First Order CI Potential Energy Curves for Ground and Excited 2π States of FO.....	34
9	Full Valence MCSCF Potential Energy Curves for Ground and Excited States for FO.....	35
10	$X^2\pi$ Dipole Moment.....	36
11	Conformations of $SO_2 \cdot H_2O$ complexes.....	50
12	Conformations of $SO_2 \cdot H_2O$ complexes including some minimum energy geometry results.....	51
13	Conformations of multiple-water complexes of SO_2	52

COMPUTATIONAL SOLUTION OF ATMOSPHERIC CHEMISTRY PROBLEMS

By

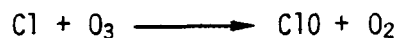
Jawed A. Jafri¹ and R. L. Ake²

INTRODUCTION

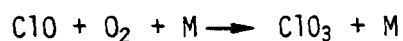
Extensive studies were carried out on problems of interest in atmospheric chemistry during the grant period. In addition to several minor projects, four major projects were carried out during the course of this research and are described in the following sections.

I. THEORETICAL STUDIES OF GROUND AND LOW-LYING EXCITED STATES OF ClO₂

Chlorine introduced into the atmosphere as a result of natural or anthropogenic processes reacts with ozone via



and



Detailed computations were carried out on the ClO₂ molecule. Ground and several low-lying excited-state potential energy curves for the doublet and quartet states in A' and A'' symmetries were calculated. The potential energy curves and other properties computed for various states were used

¹NASA Langley Research Center, Hampton, Virginia 23665

²Associate Professor, Department of Chemical Sciences, Old Dominion University, Norfolk, Virginia 23508.

to determine the nature of bonding between the Cl and O₂ fragments, the wavelengths of the solar spectrum which would cause photolysis, and the photolysis products. The results of this investigation were published in the Journal of Chemical Physics. A reprint of the article detailing and describing the results is included in the Appendix.

Investigations were carried out on the other product, ClO₃. Double zeta or better quality basis sets with polarization functions were employed. ClO₃ with this basis became too large to handle with the software programs available at that time. SCF calculations were carried out at several geometries to find the equilibrium geometry, but no binding was obtained at this level. Some GVB calculations were also carried out, but these calculations were very large and also expensive. In order to study this system properly, large scale MCSCF and CI calculations are needed together with several parameter optimizations, and since these needs exceeded the resources at that time, these calculations were postponed.

II. GROUND AND EXCITED STATE POTENTIAL ENERGY SURFACES OF THE METHYL PEROXY RADICAL, CH_3O_2

The methyl peroxy, CH_3O_2 , radical is an important intermediate in combustion processes and in the degradation of methane in the atmosphere. CH_3O_2 and subsequent products of methane degradation participate in chain reactions which are important in the production and destruction of ozone in the troposphere and stratosphere. The fractional abundance of CH_3O_2 in the atmosphere is about 10^{-11} with a lifetime of 10^3 seconds (Refs. 1, 3). Its role in the chain reaction involving methane with HO, NO, and O_2 molecules might indicate an increase in ozone concentration near the troposphere where the NO concentration may be significant (Ref. 2). The product of self reaction of CH_3O_2 radicals subsequently reacting with O_2 yields HCHO, HO_2 and CH_3O radicals and is non terminating. The absorption spectrum of CH_3O_2 in the gas phase has been studied extensively. The only theoretical ab initio work is due to Bair and Goddard (Ref. 4), who examined the ground state of CH_3O_2 to determine the equilibrium geometry using a valence double zeta basis set augmented by polarization functions in a GVB-CI scheme (Ref. 5). These computations, however, do not determine the dissociation energy or the nature of the excited states.

Work, under this grant, was carried out to calculate the ground state geometry, the dissociation energies, the nature of excited states and photolysis products using a larger basis set and a more extensive CI scheme. Two sets of computations were carried out which employed the same MCSCF procedure but different basis sets and different CI schemes. In the first set of calculations a double zeta quality Cartesian Gaussian basis set was chosen consisting of Dunning's (Ref. 6) [4s, 2p/2s] contraction of Huzinaga's (Ref. 7) (9s,5p/4s) components, with a scale factor $\zeta = 1.2$ chosen for

hydrogen's functions. The SCF solutions were obtained for the single and multiconfiguration wave functions using a modified version of the GVB programs due to Goddard and co-workers (Ref. 8). Double excitations to all antibonding orbitals from the bonding orbitals, including C-H bonds, in CH_3O_2 , were allowed in the MCSCF procedure, and the set of orbitals thus obtained was used in this first set of calculations. These "pseudo first order" CI calculations utilized CSF selection, by the A_k (Ref. 9) method, from a list generated by considering all valence double excitations from a multiple CSF reference function with the limitation that only one electron could occupy a virtual orbital. These calculations were used to carry out a preliminary search for the lowest three states in ${}^2A''$ and ${}^2A'$ symmetries.

The second set of computations on CH_3O_2 utilized the same MCSCF procedure as above with an augmented basis set. Polarization was provided by a set of d-type functions on carbon ($\alpha = 0.75$), and oxygen ($\alpha = 0.85$) and by a set of p-type functions ($\alpha = 1.0$) on the hydrogen atoms. A pseudo first order technique, similar to the one in the first set of calculations, was used to obtain a set of approximate natural orbitals. These ANO's were subsequently used to carry out a selected singles and doubles CI on the ground state. In this set of calculations, CSF's were selected from a set generated by single and double excitations into the valence and virtual space from a multiple CSF reference function, using the AK method.

The potential energies for the three lowest ${}^2A''$ and ${}^2A'$ states for various CH_3O_2 geometries, where the $R(\text{O}-\text{O})$ coordinate was varied keeping the $R(\text{C}-\text{O})$ at 2.725 bohr, are presented in Table 1.* These energies are plotted in Fig. 1.* The energies and dipole moments of the lowest ${}^2A''$ and

*Tables and figures cited in each section appear at the end of the section.

$^2A'$ state as a function of $R(CO)$ [$R(O-O) = 2.783$ bohr] are presented in Table 2 and plotted in Fig. 2. These calculations utilized a double zeta basis set and "pseudo first order" CI. The first excited state in $^2A''$ symmetry along the C-O bond stretch coordinate (Fig. 2) which should dominate the photochemistry of CH_3O_2 , exhibits a bound region near $R(C-O) = 2.75$ bohr and an avoided crossing with the third $^2A''$ state near $R(C-O) = 3.5$ bohr. Along the O-O stretching coordinate this $^2A''$ state is essentially repulsive near $R(O-O) = 2.53$, but exhibits slight bonding at longer bond lengths. The shape of the $^2A''$ surface indicates that CH_3O+O should be the principle photolysis products. If this state is slightly bound at long O-O bond lengths, a temperature dependent quantum yield for photolysis could be expected in the long wavelength tail of the absorption band for this state.

The first $^2A'$ state is bound in both the O-O and C-O bond stretching coordinates as expected on the basis of spectroscopic investigation of CH_3O_2 absorption in the near infrared. The second $^2A'$ state is repulsive in both bond stretching coordinates and exhibits a crossing with the second $^2A''$ state on the outer limbs of this state's well on the O-O bond stretching coordinate. The location of the crossing on this particular slice through the surface indicates that the resulting predissociation of $2^2A''$, CH_3O_2 to CH_3O+O should not be important. This indication, however, is not definitive due to the sparse coverage of the region and the approximations in the level of CI treatment. The excitation energy of the $2^2A'$ state in the region of the ground state equilibrium should prevent it from being significant in the atmospheric photochemistry of CH_3O_2 .

The second series of computations with more comprehensive CI treatment and larger basis set as discussed above was carried out. The energies

for the first two $^2A''$ states along the $R(O-O)$ coordinate with $R(C-O)$ fixed at 2.7483 bohr are presented in Table 3 and plotted in Fig. 3. The energy of the second $^2A''$ is lower (at long bond lengths) along the $R(O-O)$ stretching coordinate and exhibits bonding similar to that found in the "pseudo first order" calculation along that slice in this coordinate. The dissociation energy for $CH_3O_2 \rightarrow CHO_3 + O$ determined at this level of calculation is 3.36 eV.

The refined computations on the potential energy curves along the $R(C-O)$ stretching coordinate, with $R(O-O)$ fixed at 2.5606 bohr are presented in Table 4 and plotted in Fig. 4. The computations give similar results as in "pseudo first order" calculations with the avoided curve crossing between second and third $^2A''$ states near $R(C-O) = 3.2$ bohr. The calculation reported in Tables 3 and 4 utilized different approximate natural orbitals for the first and second roots. The dissociation energy for $CH_3O_2 \rightarrow CH_3 + O_2$ at this level of computation was 2.08 eV.

The potential energy curve along a 45° angle in the plane defined by the $R(C-O)$ and $R(O-O)$ coordinates is presented in Table 5 and plotted in Fig. 5. Here again, different approximate natural orbitals were employed for the first and second root calculations. The second $^2A''$ state is purely repulsive along this coordinate.

The vertical excitation energy between the $x \ ^2A'' + 1 \ ^2A'$ is computed to be 1.23 eV in the "pseudo first order" type calculations.

Table 1. Energies of the lowest ${}^2A''$ and ${}^2A'$ states of CH_3O_2 as a function of $R(\text{O}-\text{O})$; $R(\text{C}-\text{O})$ fixed at 2.725 bohr.

$R(\text{O}-\text{O})$	State	E_1	E_2	E_3
2.1505	${}^2A''$	-189.298021	-188.984950	-188.927101
	${}^2A'$	-189.239457	-188.974894	-188.968584
2.430	${}^2A''$	-189.366776	-189.137986	-189.006940
	${}^2A'$	-189.323150	-189.108858	-189.051324
2.530	${}^2A''$	-189.375718	-189.170388	-189.060038
	${}^2A'$	-189.336555	-189.137441	-189.102755
2.680	${}^2A''$	-189.380272	-189.209729	-189.121958
	${}^2A'$	-189.347146	-189.167850	-189.161750
2.783	${}^2A''$	-189.379000	-189.227709	-189.153899
	${}^2A'$	-189.349894	-189.191495	-189.182926
2.900	${}^2A''$	-189.375016	-189.242442	-189.181881
	${}^2A'$	-189.349249	-189.217065	-189.194490
3.036	${}^2A''$	-189.368279	-189.253157	-189.205724
	${}^2A'$	-189.347488	-189.239335	-189.203314
3.289	${}^2A''$	-189.353644	-189.260269	-189.230523
	${}^2A'$	-189.339151	-189.264805	-189.212428
3.619	${}^2A''$	-189.336507	-189.267475	-189.251220
	${}^2A'$	-189.327569	-189.281986	-189.217849
3.796	${}^2A''$	-189.329485	-189.264481	-189.252198
	${}^2A'$	-189.324086	-189.288061	-189.216604
∞	${}^2A''$	-189.309762	-189.295345	-189.224714
	${}^2A'$	-189.304290	-189.302305	-189.216360

Table 2. Energies of the lowest ${}^2A''$ and ${}^2A'$ states of CH_3O_2 as a function of $R(\text{C-O})$; $R(\text{O-O})$ fixed at 2.783 bohr.

$R(\text{C-O})$	State	E_1	E_2	E_3
2.4425	${}^2A''$	-189.350966	-189.213618	-189.120739
	${}^2A'$	-189.321927	-189.165722	-189.161895
2.60	${}^2A''$	-189.371913	-189.226331	-189.151162
	${}^2A'$	-189.342519	-189.183436	-189.179728
2.725	${}^2A''$	-189.379219	-189.228451	-189.158422
	${}^2A'$	-189.349362	-189.190420	-189.183653
2.85	${}^2A''$	-189.380861	-189.226953	-189.160862
	${}^2A'$	-189.350579	-189.191848	-189.183186
2.998	${}^2A''$	-189.378283	-189.221670	-189.159368
	${}^2A'$	-189.347174	-189.188517	-189.178544
3.270	${}^2A''$	-189.365512	-189.207281	-189.154780
	${}^2A'$	-189.332228	-189.175355	-189.164866
3.543	${}^2A''$	-189.347680	-189.191854	-189.168744
	${}^2A'$	-189.312382	-189.156824	-189.147050
3.815	${}^2A''$	-189.329582	-189.200697	-189.172280
	${}^2A'$	-189.294127	-189.164362	-189.130020
∞	${}^2A''$	-189.315773	-189.089019	-189.981690

Table 3. Energies (in Hartrees) of the first two $^2A''$ states along the R(O-O) stretching coordinate with R(C-O) = 2.7483 bohr.

R (O-O)	E_1^*	E_2^{**}
2.411	-189.627009	-189.360728
2.5606	-189.634754	-189.399470
2.711	-189.629232	-189.429652
2.80	-189.624619	-189.438978
2.861	-189.619795	-189.460298
3.00	-189.609292	-189.448384
3.30	-189.583719	-189.476526
3.80	-189.554940	-189.444410
∞	-189.511096	

*Energies calculated using approximate natural orbitals for the $^2A''$ state.

**Energies calculated using approximate natural orbitals for the second $^2A''$ state.

Table 4. Energies (in Hartrees), for the first two ${}^2A''$ states in the R(C-0) stretching coordinate. R(0-0) was fixed at 2.5606 bohr.

R(C-0)	E_1^*	E_2^{**}
2.598	-189.631742	-189.408465
2.748	-189.634754	-189.399470
2.898	-189.629929	-189.395334
3.10	-189.615957	-189.380685
3.30	-189.587609	-189.363211
3.60	-189.575821	-189.402720
3.90	-189.556006	-189.438198

* Energies calculated using approximate natural orbitals for X^2A'' state.

** Energies calculated using approximate natural orbitals for $2^2A''$ state.

Table 5. Energies (in Hartrees) of the X^2A'' and $2^2A''$ states along the stretching coordinate along a 45° angle through the plane defined by $R(C-O)$ and $R(O-O)$ stretches. The first and second root $^2A''$ states employed approximate natural orbitals determined separately.

R	E_1	E_2
3.5443	-189.627012	-189.363965
3.6033	-189.632922	-189.380388
3.7583	-189.634754	-189.399470
3.9133	-189.632372	-189.415834
3.9683	-189.626890	-189.422632
4.1803	-189.606836	-189.425222

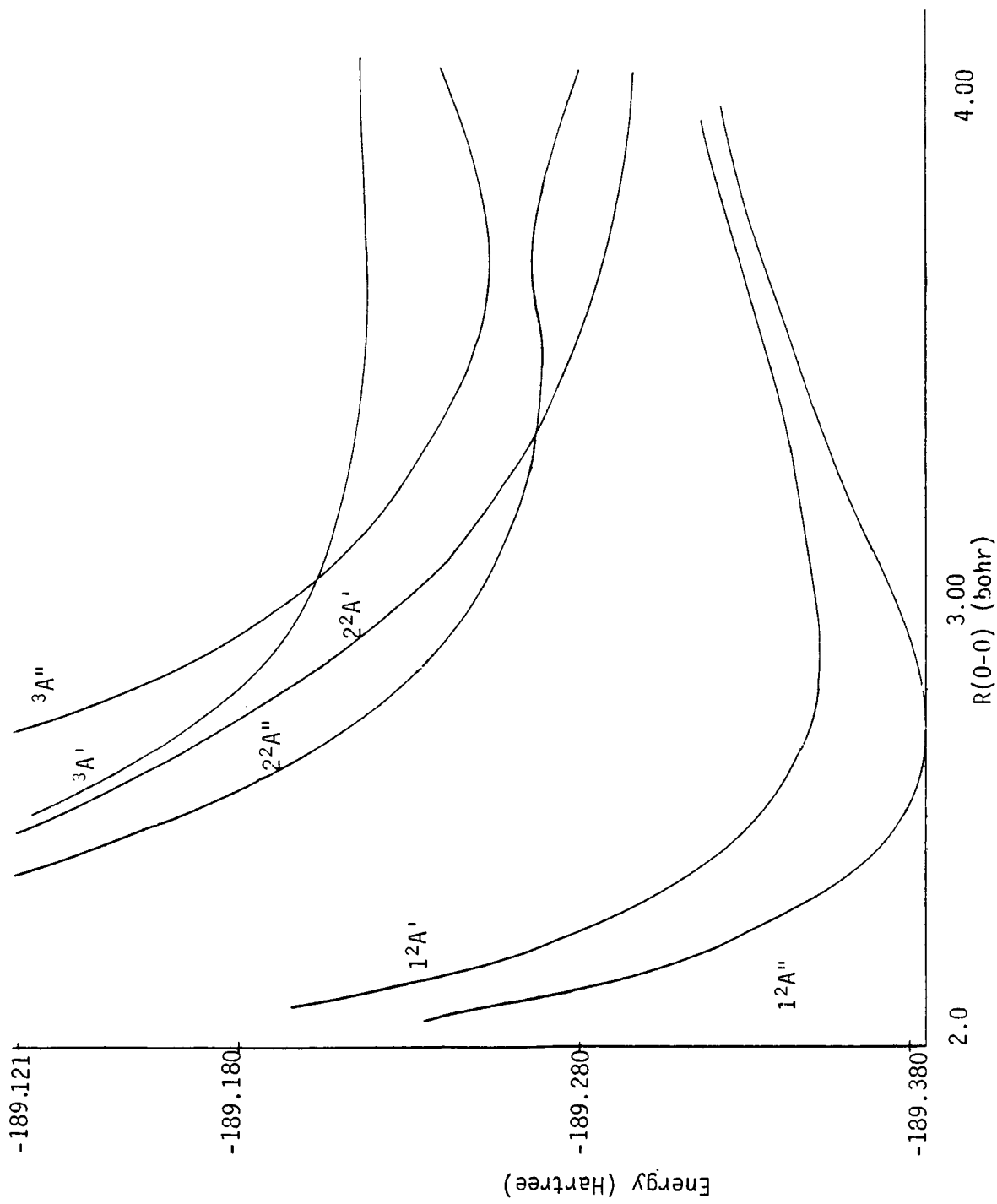


Figure 1. Potential energy of the lowest $2A''$ and $2A'$ states of CH_3O_2 along the $R(O-O)$ coordinate. The calculations used a double zeta basis and selected "pseudo first order" CI. $R(C-O)$ fixed at 2.725 bohr.

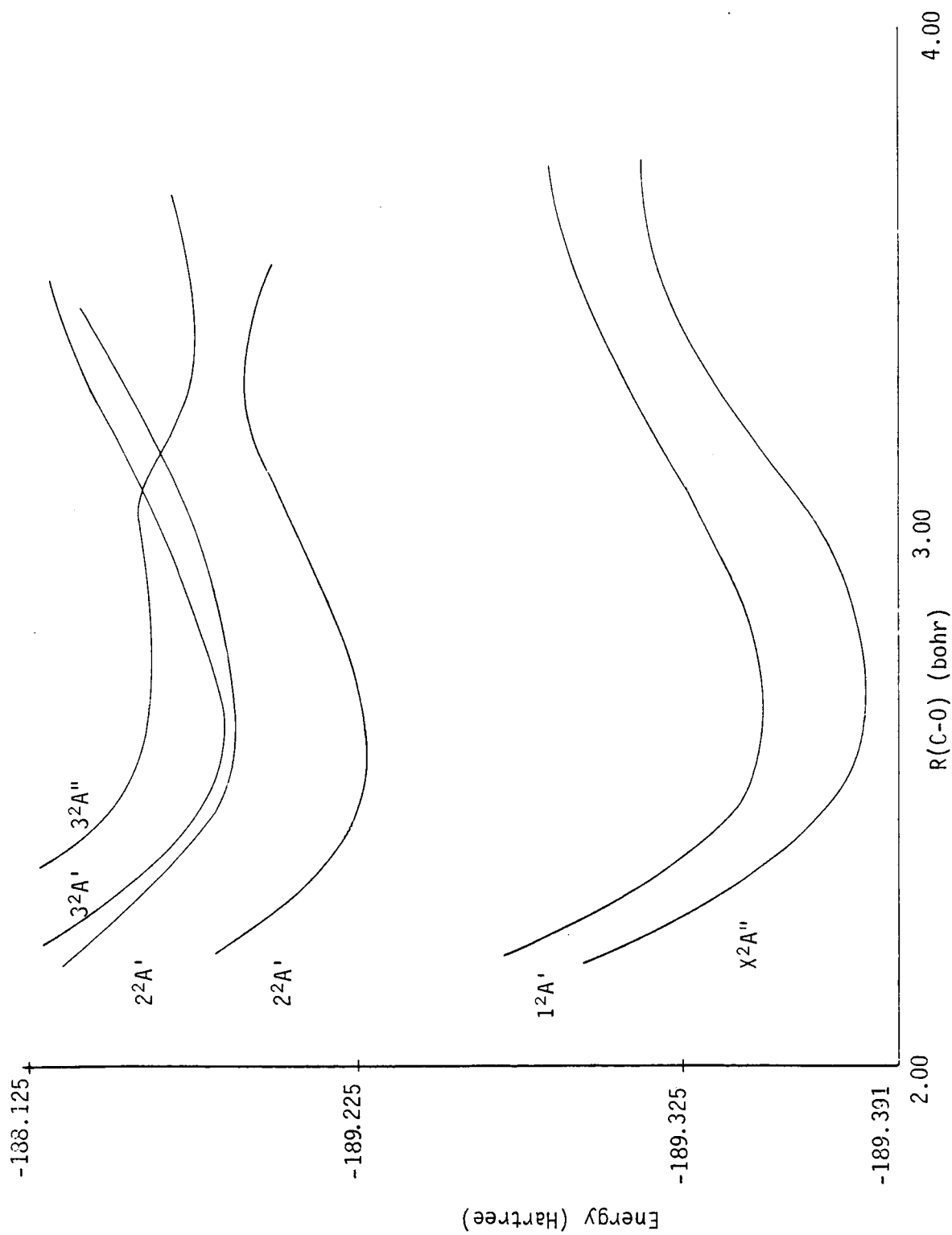


Figure 2. Potential energy of the lowest $2A''$ and $2A'$ states of the CH_3O_2 radical along the $R(\text{C-O})$ coordinates. The calculations used a double zeta basis and selected "pseudo first order" CI. $R(0-0)$ fixed at 2.783 bohr.

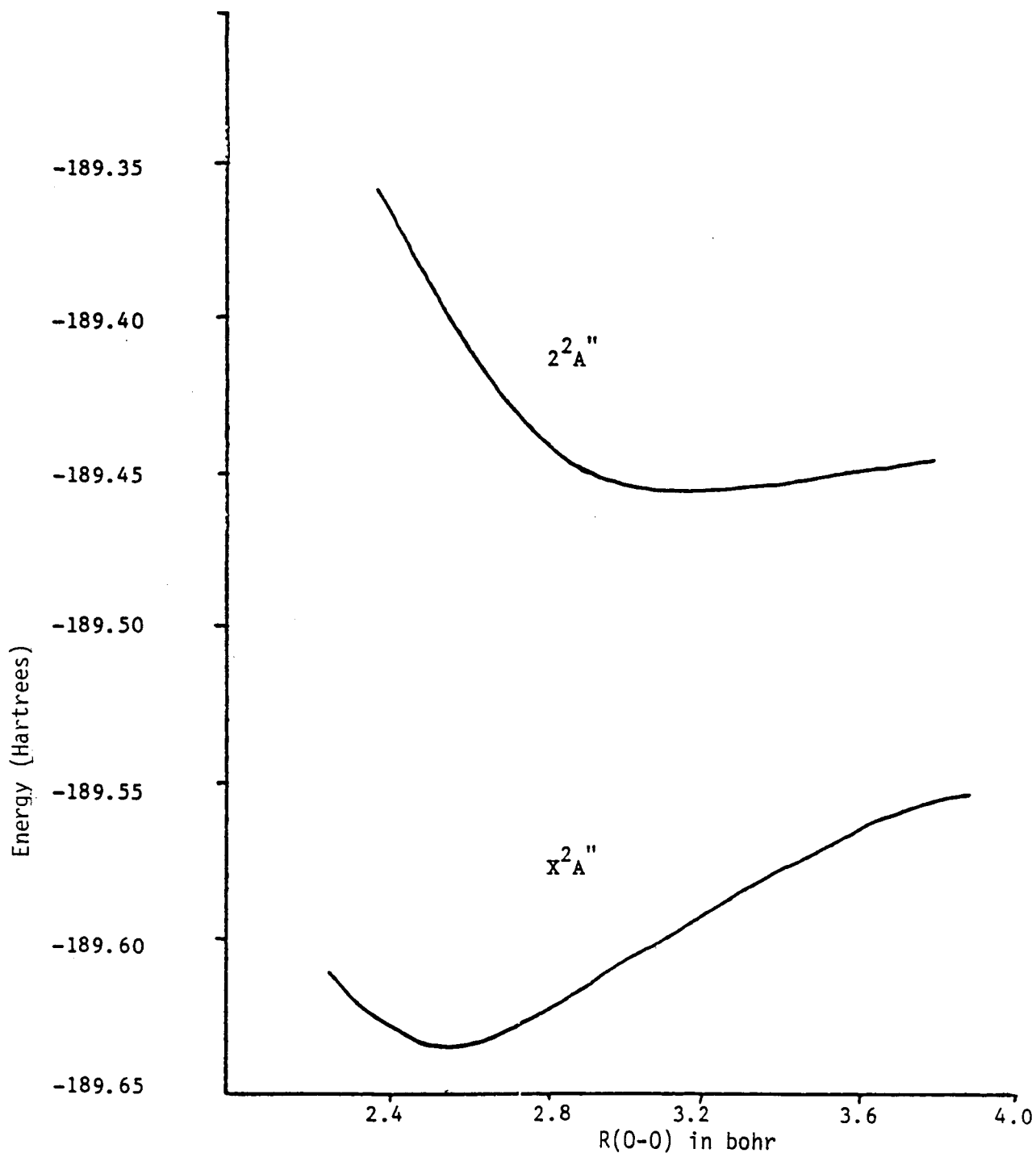


Figure 3. Potential energy of the X^2A'' and $2^2A''$ states of CH_3O_2 along the $R(\text{O}-\text{O})$ coordinate. The calculations used a double zeta basis augmented by polarization functions and a selected single and double CI in approximate natural orbital basis. $R(\text{C}-\text{O})$ fixed at 2.7483 bohr.

ORIGINAL PAGE IS
OF POOR QUALITY

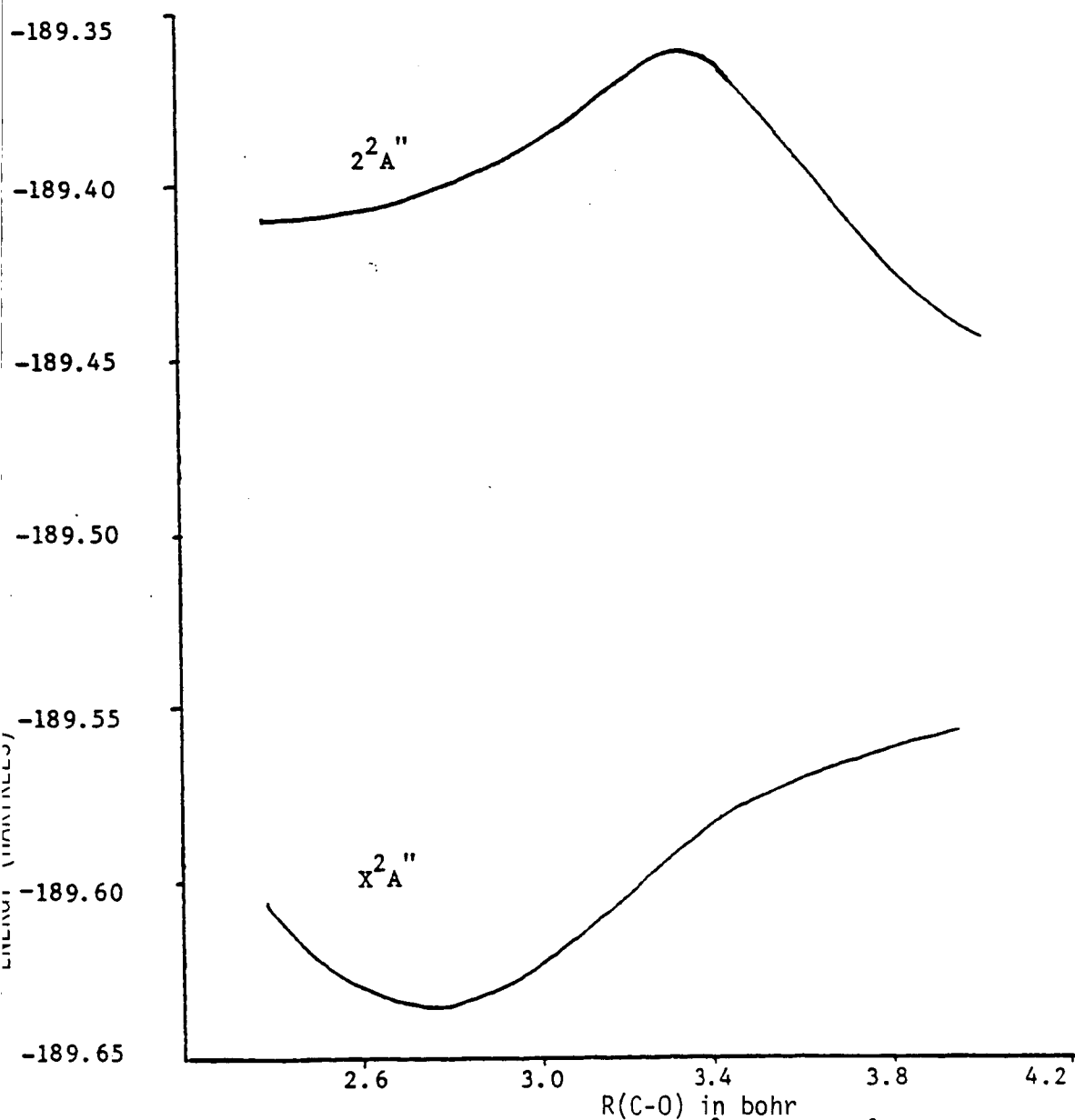


Figure 4. Potential energy of the $\text{X}^2\text{A}''$ and $2^2\text{A}''$ states of CH_3O_2 along the $\text{R}(\text{C}-\text{O})$ coordinate. The calculations used a double zeta basis augmented by polarization functions and selected "single and double" CI in approximate natural orbital basis. $\text{R}(\text{O}-\text{O})$ fixed at 2.5606 bohr.

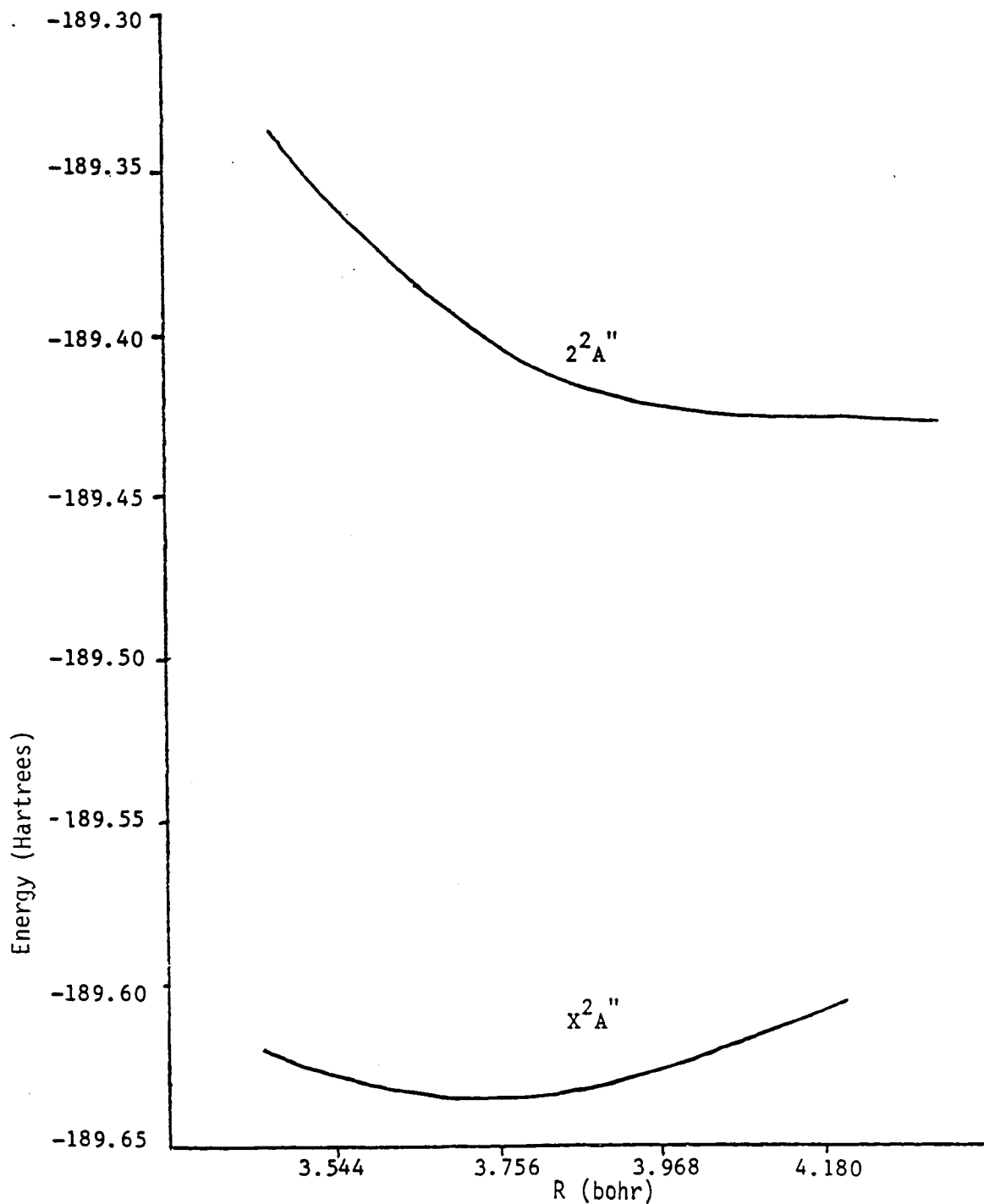


Figure 5. Potential energy of X^2A'' and $2^2A''$ states of CH_3O_2 along 45° angle in the plane defined by $R(C-O)$ and $R(O-O)$ coordinates. The calculations used a double zeta basis augmented by polarization functions and selected singles and doubles CI in approximate natural orbital basis.

III. ELECTRONIC STATES OF THE FO RADICAL.

The ground and lower excited states of the FO radical have been investigated using a large basis set with MCSCF and CI techniques. FO has long been an elusive molecule. Direct evidence of its existence was not obtained until 1964 when Arkell, Reinhard and Larson (Ref. 10) detected the IR band at 1028 cm^{-1} in an argon matrix containing the photolysis products of F_2O . Andrews (Ref. 11) subsequently studied the fundamental bands using Raman spectroscopy of F_2O photolysis products in an Argon matrix. Early estimates of dissociation energy of FO ranged from 24 Kcal/mole based on direct evidence from electron impact studies to 46 Kcal/mole inferred from the thermolysis of F_2O . Later experiments produced values for the dissociation energy of FO as high as 59 Kcal/mole.

O'Hare and Wahl (Ref. 12) and Lathan et. al (Ref. 13) have reported Hartree Fock calculations on the ground state of the FO radical. Langhoff, et. al (Ref. 16) studied the $X^2\pi$ potentials and dipole moment functions for FO at the CASSCF, externally contracted CI and MRCI(SD) levels using double zeta plus polarization and extended Gaussian basis sets. No experimental or theoretical results are available for the excited states of FO radical.

Ab initio calculations using an accurate basis and including electron correlation, on the ground and excited of FO radical were carried out. MCSCF and first order CI calculations have been carried out for the ground and excited states, and selected singles and doubles CI for the ground state obtaining potential energy curve, dipole moment curves, and transition moments between various excited states and $X^2\pi$ ground state. The intensities of the vibrational transitions have been obtained in order to provide a basis for infrared measurements of the concentration of FO in either the

laboratory or the upper atmosphere where the radical may be produced by the photochemistry of fluoro-carbons.

The basis set used in the ground state and all excited state calculations was a triple zeta contraction of Van Dujneveldt's (Refs. 14, 15) (11S,7p) valence augmented by two sets of d functions. The exponents for the d-type functions on the oxygen atom were 2.091 and 0.6194 and on the fluorine atom were 2.214 and 0.656. This basis set yields an SCF energy for the $X^2\pi$ state at 2.5 bohr internuclear distance which is 3×10^{-4} Hartrees higher than O'Hare and Wahl's near Hartree-Fock value.

The initial orbitals were obtained by carrying out a GVB calculation where the excitation involved replacement of the FO bonding orbital with the antibonding orbital. The orbitals arising principally from combinations of the atomic 1s orbitals were frozen for all subsequent calculations. The orbitals were further optimized by carrying out a full valence MCSCF calculation using a general second order MCSCF technique developed by Lengsfeld (Ref. 16). These calculations were carried out in C_{2v} symmetry. The virtual orbitals of Δ symmetry which arise from the d-orbitals were omitted from the full valence MCSCF calculations in order to prevent their being mixed with the orbitals of the π symmetry. These Δ type orbitals were included in the subsequent CI calculation. The CI calculations utilized the full symmetry of the molecule. The ground state of the FO radical was investigated at two levels of CI treatment. The first order CI treatment is generally regarded as providing accurate one electron properties. This was followed by an A_k (Ref. 8) selected single and double excitation, multi-reference (SD-CI) treatment in order to determine the degree of convergence of the dissociation energy. To ensure a uniform treatment throughout the potential energy surface, important CSF's were selected from the MCSCF

results at the equilibrium geometry and for larger separation of the O and F atoms. The union of these two sets of important CSF's were used across the potential energy curve. The vibrational Schrödinger equation was integrated using the calculated potential energy curve.

The matrix elements of the dipole moment operator were calculated in order to determine the vibrationally averaged dipole moment and vibrational intensities. Separate MCSCF calculations were carried out for each excited state investigated. Full valence and first order computations were carried out for the full curve on $2^2\pi$ and $3^2\pi$ excited states and at the ground state equilibrium geometry for other doublet and quartet states. These results are presented in Tables 6-16, and are plotted in Figs. 6-10.

The potential energy curve for the low lying excited states of FO radical were found to be repulsive, and an avoided crossing was found between $2^2\pi$ and $3^2\pi$ states near 3.3 bohr. The repulsive nature of the excited states provides an explanation for the failure of experiments intended to detect band spectrum for the FO radical. The intersection between $2^2\pi$ and 3^2P states may lead to the production of small amounts of atomic oxygen in the 1D state if the FO radical is in fact produced and photodissociated in the upper atmosphere. The calculated excitation energies (F.O. CI) indicate that the absorption continuum due to the second 2π state should have a maximum at approximately 6.4 eV. This absorption maximum due to the weaker transition of the $^2\Delta$ and $^2\Sigma^-$ state should occur at about 5.9 eV, and the weak absorption due to the $^2\Sigma^+$ state should peak at about 6.6 eV. These spectra should combine to yield a relatively broad and featureless continuum.

The dipole moment curve for the ground state crosses zero near 2.5 bohr separation and the magnitude of the dipole moment operator supports the

conjecture that the failure of the experimental attempts to measure the epr spectrum was due to a small dipole moment. The dipole moment for the $2 \ 2\pi$ state goes to zero when the $x^2\pi$ dipole goes through a maximum. The theoretical dissociation energy and vibrational frequencies agree well with the available experimental measurements.

Table 6. Nature of Ground State Wave function for F0 at Various Levels of Computation.

<u>Occupation^(a)</u>	<u>Coefficient at MCSCF level</u>	<u>Coefficient at FOCI^(b) level</u>	<u>Coefficient at SD^(c)-Selected CI level</u>
(core) 5σ ² 1π ⁴ 2π ³	0.9671	0.9477	0.9484
(core) 5σ ² 1π ³ 2π ⁴	0.1141	0.1599	0.0903
(core) 5σ 6σ 1π ³ 2π ⁴	0.1189	0.1103	0.0798
(core) 6σ ² 1π ⁴ 2π ³	0.1762	0.1403	0.1409

R(F-0) = 2.6 bohr

(a) Only one spin coupling was important for each occupation. The occupation is used to represent the most important CSF for that occupation.

(b) First Order CI

(c) Singles and Doubles selected CI

Table 7. F0 Ground State Energies (Hartrees) as a Function of Internuclear Separation at Various Levels of Computation.

<u>R(F-0) (bohr)</u>	<u>MCSCF</u>	<u>FOCI</u>	<u>Selected S-D CI</u>
2.10	-174.180888	-174.291148	
2.30	-174.236725	-174.349259	-174.584322
2.35	-174.244387	-174.357284	-174.592071
2.40	-174.250186	-174.363248	-174.597805
2.45	-174.255001	-174.370319	-174.603071
2.50	-174.257808	-174.370319	-174.605677
2.55	-174.259504	-174.371665	-174.607192
2.60	-174.259872	-174.371889	-174.608246
2.65	-174.260276	-174.371350	-174.607299
2.70	-174.259651	-174.369992	-174.606288
2.75	-174.258521	-174.368007	-174.604676
2.80	-174.253093	-174.365510	-174.602483
2.85	-174.256992	-174.362598	-174.600048
2.95	-174.250874	-174.355873	-174.594218
3.00	-174.248560	-174.352177	-174.593418
3.05	-174.246202	-174.348424	-174.587705
3.10	-174.243845	-174.344577	-174.584321
3.30	-174.235069	-174.329412	-174.570593
3.70	-174.223517	-174.305429	-174.547950
4.10	-174.218899	-174.292375	-174.533233
4.50	-174.217370	-174.286567	-174.524961
4.90	-174.216870	-174.284135	
6.50	-174.216860	-174.282520	-174.515506

Table 8. Energies (Hartrees) for the 2π Ground and Excited States of FO at MCSCF Level.

<u>R(F-0) (bohr)</u>	<u>$x^2\pi$</u>	<u>$2^2\pi$</u>	<u>$3^2\pi$</u>	<u>$4^2\pi$</u>
2.1	-174.180888			
2.3	-174.236725			
2.5	-174.257808	-174.00420		
2.6	-174.259872	-174.03239	-173.862516	
2.7	-174.259651	-174.05410	-173.915170	
2.9	-174.253093	-174.0839	-173.99278	
3.0	-174.248560	-174.094221	-174.030919	
3.1	-174.243845	-174.102334	-174.062809	
3.2		-174.108807	-174.089343	-174.062341
3.3	-174.235069	-174.11390	-174.109419	-174.076966
3.4		-174.129959	-174.117929	-174.08863
3.5		-174.14516	-174.121464	-174.097914
3.6		-174.157729		-174.105293
3.7	-1714.223517	-174.16810	-174.128365	-174.11162
4.1	-174.218899	-174.20650	-174.131681	
4.9	-174.216870	-174.21180	-174.134974	
6.5	-174.216860	-174.214917	-174.135980	

Table 9. Coefficients of Important CSF's for $2^2\pi$ and $3^2\pi$ States of F0 as a Function of Internuclear Separation.

		R(F-0) (bohr)			
Occupation ^a		<u>3.1</u>	<u>3.3</u>	<u>3.4</u>	<u>3.5</u>
SCF Config.	$2^2\pi$	-0.114	-0.041	-0.023	-0.025
	$3^2\pi$	-0.023	-0.005	0.076	0.103
$(\pi_x, \pi_y^*) \rightarrow \sigma^*$	$2^2\pi$	-0.023	-0.036	0.328	-0.310
	$3^2\pi$	-0.287	-0.166	0.026	-0.040
$(\pi_y, \pi_x^*) \rightarrow \sigma^*$	$2^2\pi$	0.003	0.024	0.796	0.797
	$3^2\pi$	0.857	0.677	-0.185	-0.040
$(\pi_x, \pi_y) \rightarrow \sigma^*$	$2^2\pi$	-0.005	0.001	0.456	0.465
	$3^2\pi$	0.412	0.364	-0.116	-0.036
$\sigma \rightarrow \sigma^*$	$2^2\pi$	0.775	0.730	0.017	0.010
	$3^2\pi$	-0.035	-0.437	0.703	0.695
$\sigma \rightarrow \sigma^*$ $\pi \rightarrow \pi^*$	$2^2\pi$	0.087	0.236	0.009	0.009
	$3^2\pi$	-0.023	-0.173	0.254	0.276
$(\sigma)^2 \rightarrow (\sigma^*)^2$	$2^2\pi$	0.519	0.549	0.010	0.004
	$3^2\pi$	-0.027	-0.344	0.504	0.524
$(\sigma)^2 \rightarrow (\sigma^*)^2$ $\pi \rightarrow \pi^*$	$2^2\pi$	-0.115	-0.155	-0.001	0.010
	$3^2\pi$	-0.080	0.168	-0.169	-0.189

a. In each case, only one spin coupling was important for each occupation. The occupations are therefore used to represent the dominant CSF.

Table 10. First Order CI Energies (Hartrees) for π Excited States of F0.

<u>R(F-0) (bohr)</u>	<u>$x2\pi$</u>	<u>22π</u>	<u>32π</u>
2.6	-174.371889	-174.13771766	-174.9471872
3.0	-174.352177	-174.18901197	-174.10948514
3.2		-174.1970095	-174.1625669
3.3	-174.305429	-174.1991699	-174.18238933
3.4		-174.2007387	-174.1982876
3.5		-174.2141748	-174.20198083
3.6		-174.2259253	-174.20198083
6.5	-174.282520	-174.2813276	-174.1983615

Table 11. Full Valence Excited State Wave Functions of F0.

State	Occupation	Component
$2\Sigma^-$	(core) $5\sigma^2 6\sigma 1\pi^4 2\pi^2$	major
	(core) $5\sigma^2 6\sigma 1\pi^3 2\pi^3$	minor
$2\Sigma^+$	(core) $5\sigma 1\pi^4 2\pi^4$	minor
	(core) $5\sigma^2 6\sigma 1^4 2\pi^2$	major
	(core) $5\sigma^2 6\sigma 1\pi^3 2\pi^3$	major
2Δ	(same occupation as $2\Sigma^+$)	
$4\Sigma^-$	$5\sigma^2 6\sigma 1\pi^3 2\pi^3$	major
	$5\sigma^2 6\sigma 1\pi^3 2\pi^3$	minor
	$5\sigma^2 6\sigma 1\pi^4 2\pi^2$	minor

Table 12. MCSCF Energies (Hartrees) for $4\Sigma^-$, $2\Sigma^-$, $2\Sigma^+$, and 2Δ Excited States of F_0 .

R(F_0) (bohr)	State				
	$4\Sigma^-$	2Δ	$2\Sigma^+$	$2\Sigma^-$	$\times 2\pi$
2.5	-174.0822	-174.0043	-173.9901	-174.9963	-174.2578
2.6	-174.1172	-174.0423	-174.0244	-174.0361	-174.2599
2.6*	-174.2406	-174.1597	-174.1302	-174.1532	-174.3719
2.7	-174.1434	-174.0719	-174.0556	-174.0700	-174.2596
2.9	-174.1770	-174.1139	-174.1015	-174.1166	-174.2530
3.3	-174.2043	-174.1631	-174.1583	-174.1688	-174.2350
3.7	-174.2124	-174.1908		-174.1953	-174.2235
4.1	-174.2154	-174.2048			-174.2188
4.5	-174.2171	-174.2112			-174.2173
4.9	-174.2181	-174.2140			-174.2168

*Energies from first order CI calculations.

Table 13. Expectation Values of the Dipole Moment^a of F0.

<u>Type^b</u>	<u>v</u>	<u><M></u>
A	0	.048
	1	.065
	2	.072
	3	.094
B	0	.015
	1	.017
	2	.025
	3	.033

a. In atomic units (1au = 2.5416 Debye)

b. Calculation A used the potential and dipole moment curve from the selected SD-CI treatment. Calculation B used first order CI values for both the potential and the dipole moment.

Table 14. Dipole Moments of $X^2\pi$ and the 2π States of F0 at Full Valence CI Level.

<u>R(F-0) (bohr)</u>	<u>$X^2\pi$</u>	<u>2π</u>
2.5	-.0245	-.9056
2.6	.0418	-.7170
2.9	.1234	-.7853
3.05	.1430	-.6387
3.30	.1386	-.3477
3.4		-0.531
3.50		-0.0484
3.70	0.0880	-.0397
4.1	0.0461	-.0249

Table 15. SD-CI Vibrational Frequencies and Transitions Moments^a.

<u>v</u>	<u>$\Delta G_{j,j-1}$ (cm⁻¹)</u>	<u>$T(\Delta v = 1)$</u>
0	0	
1	941(1044)	.012 (.013)
2	930(1035)	.022 (.025)
3	904(1014)	.033 (.036)
4	885(991)	.040 (.047)

- a. Calculated using the potential obtained from the SD-CI. The intensities are in atomic units (1au = 2.5416 x 10⁻¹⁸ esu cm⁻¹). The values given in parenthesis were obtained using the dipole, moment and potential energy curves from the first order calculations. The $\Delta v = 1$ transition moments are listed with the upper vibrational state for each transition.

Table 16. Transition Moments of F_0 at Full Valance Level of Computation at 2.60 Bohr Internuclear Separation.

$$2\Sigma^- \rightarrow x2\pi \quad T = -0.082115$$

$$2\Delta \rightarrow x2\pi \quad T = + 0.027329$$

$$2\Sigma^+ \rightarrow x2\pi \quad T = 0.17517$$

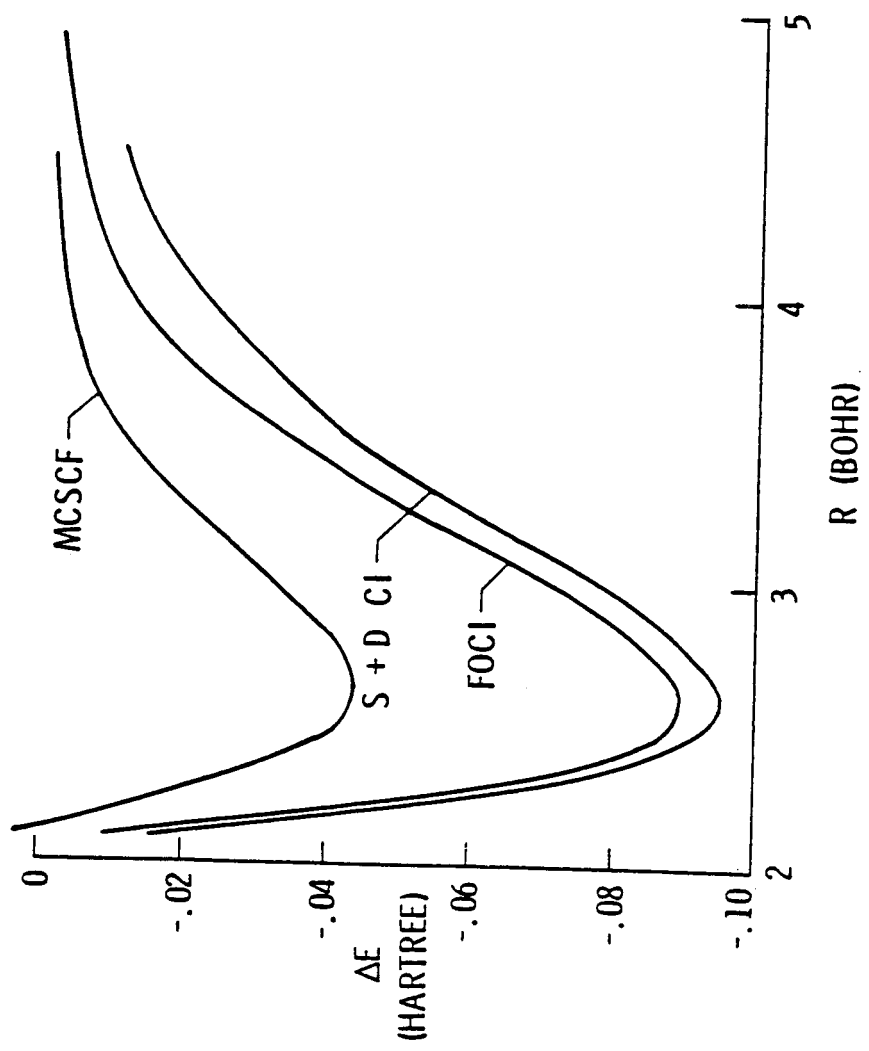


Figure 6. Potential energy curves for the $x^2\pi$ state of F_0 .

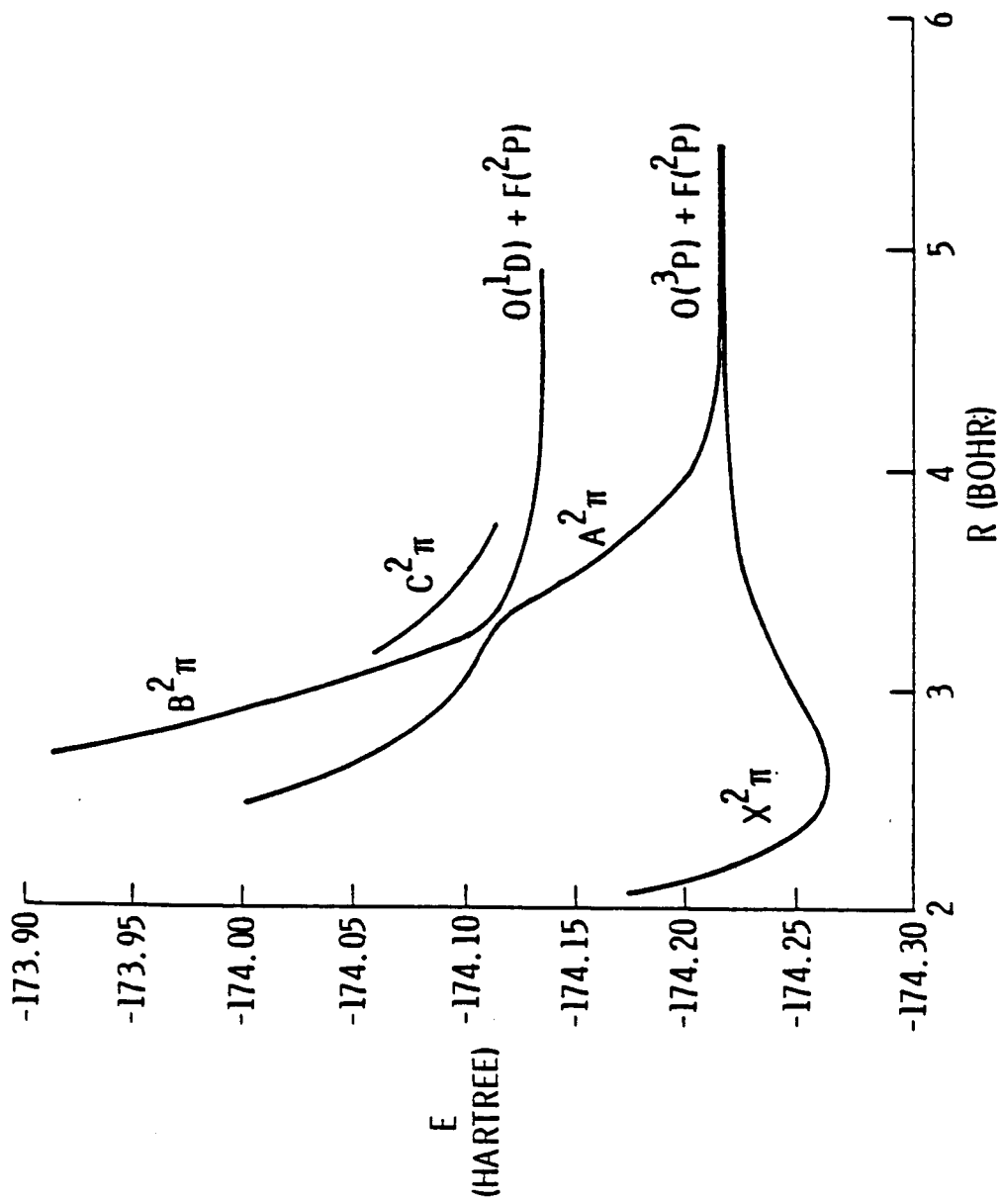


Figure 7. Full valence MCSCF Potential Energy Curves for Ground and Excited $2-\pi$ States of F_0 .

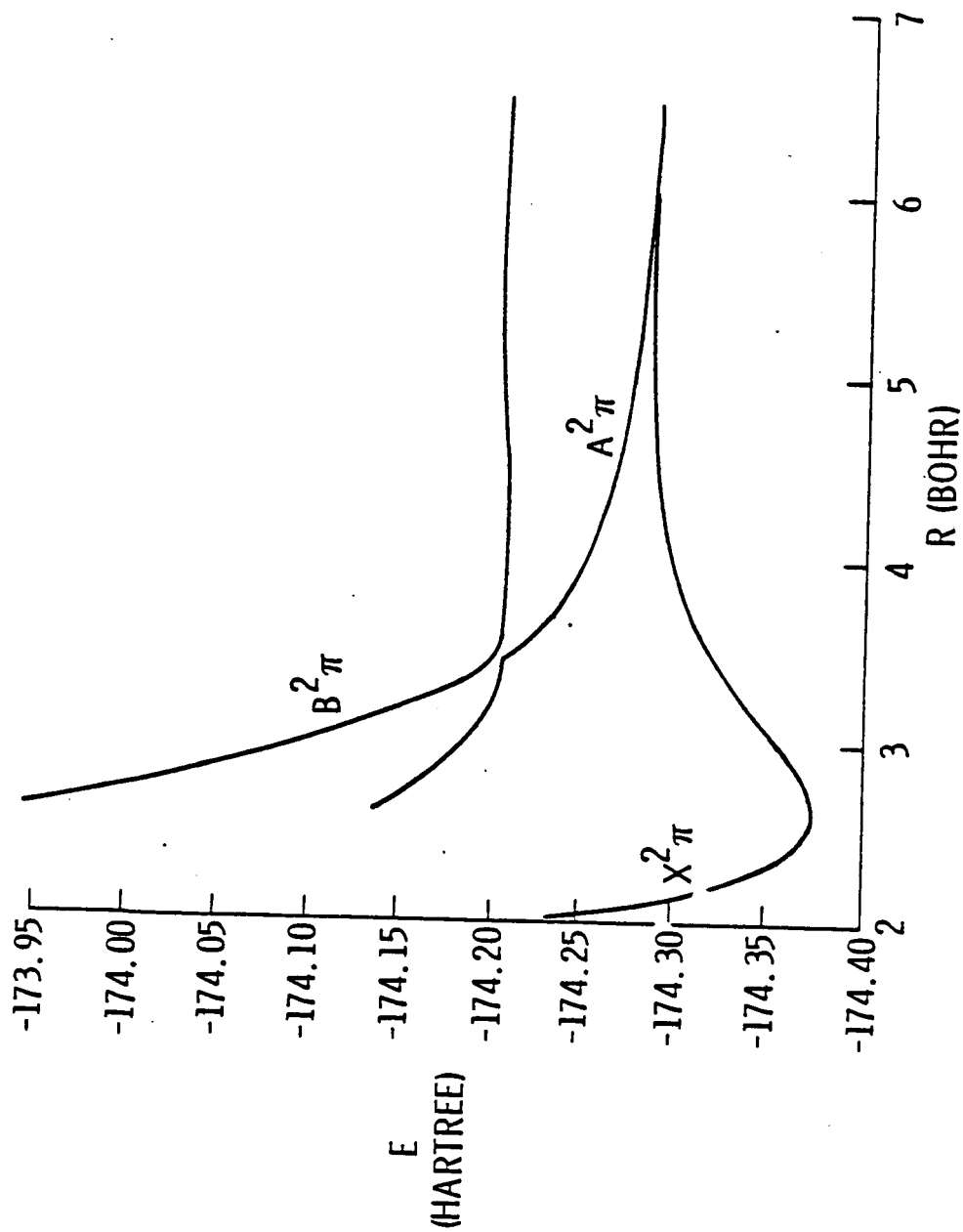


Figure 8. First Order CI Potential Energy curves for Ground and Excited 2π States of FO.

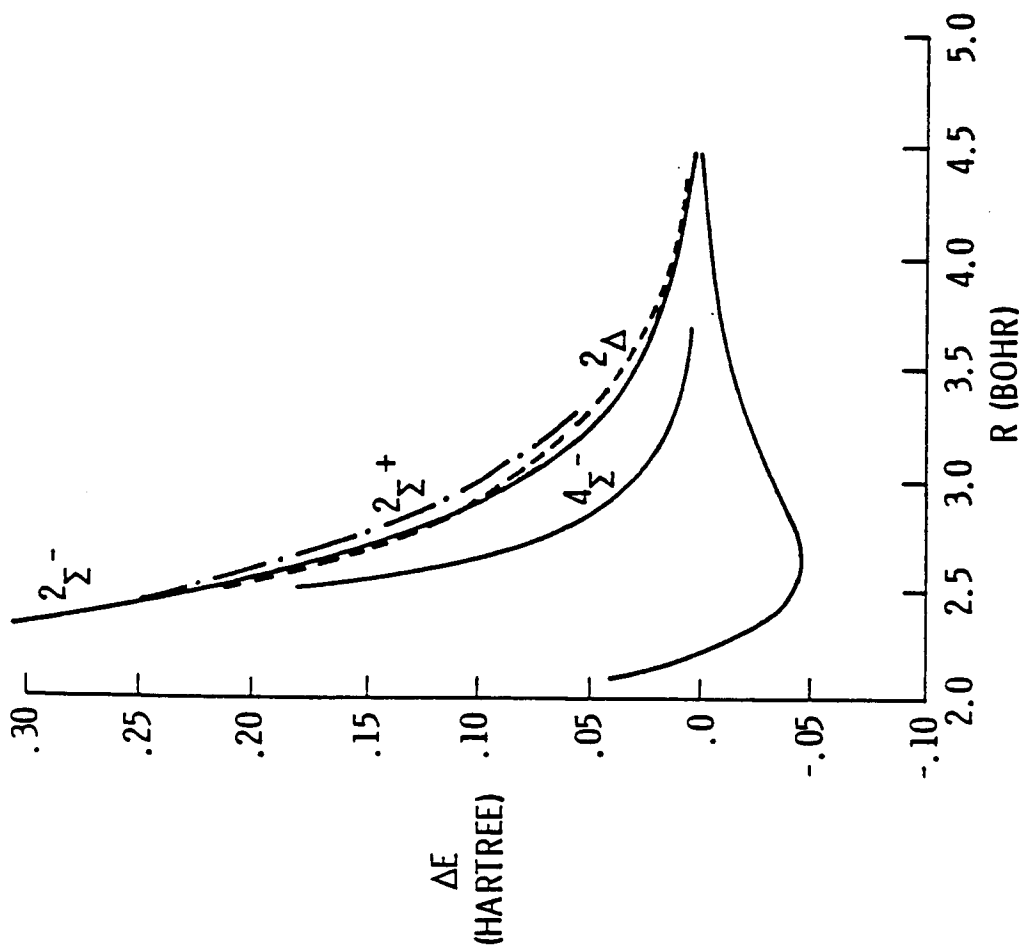


Figure 9. Full Valence MCSCF Potential Energy Curves for Ground and Excited States for F_0 .

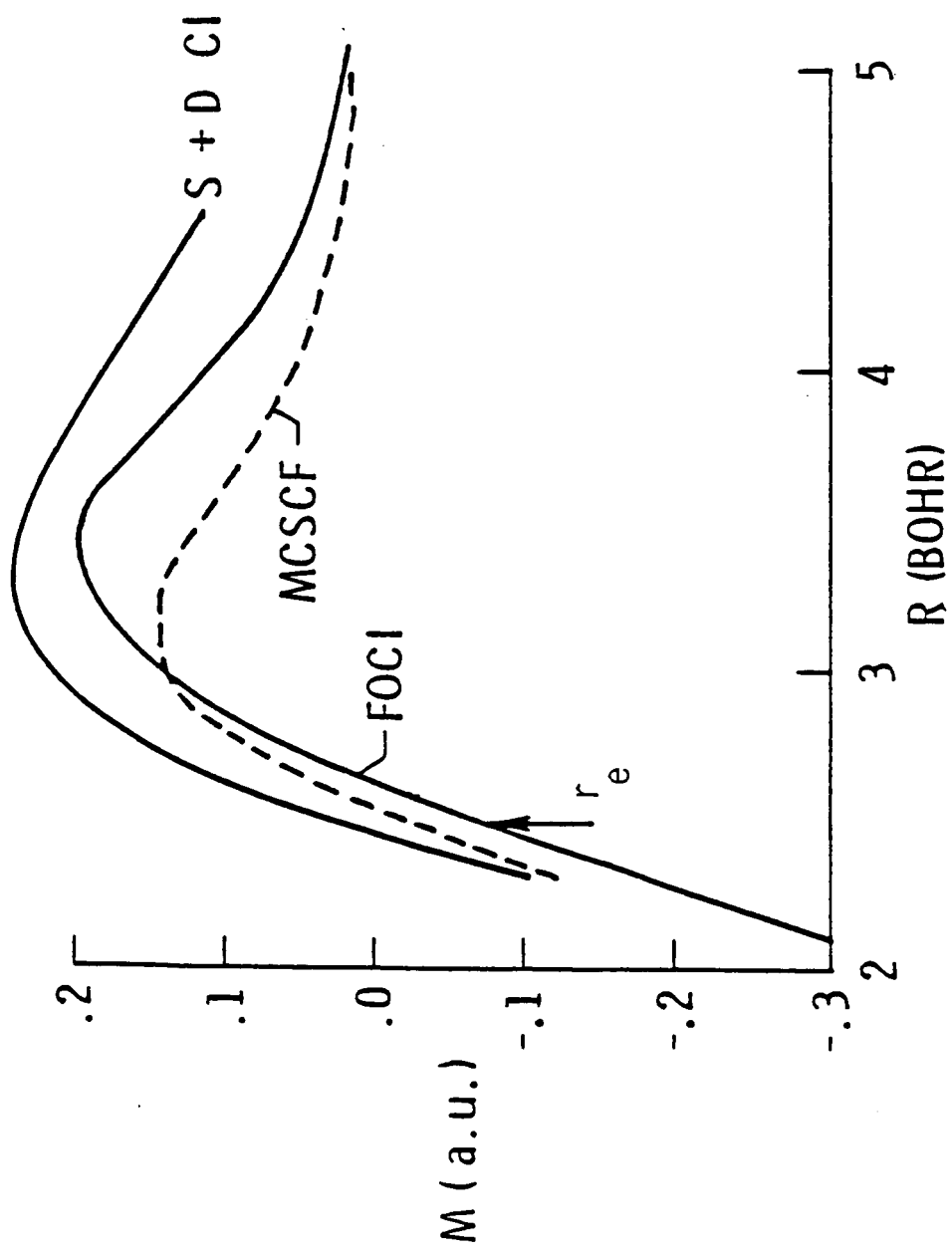


Figure 10. $x^2\pi$ Dipole Moment.

IV. THEORETICAL STUDIES OF $\text{SO}_2 \cdot (\text{H}_2\text{O})_n$ COMPLEXES

The oxidation of SO_2 is an important chemical process. The phenomenon of "acid rain" involves the oxidation of sulfur containing species including SO_2 to form SO_3 . Hydration is involved to give H_2SO_4 which in turn is ultimately precipitated as sulfates (Ref. 17). The influence which water plays on the kinetics of oxidation is less clear. However, Rees noted a 4.7×10^3 fold increase in the formation of H_2SO_4 from SO_2 in the 283% relative humidity of a smog chamber over that in the absence of water (Ref. 18). SO_2 may also act as the nucleation center for aerosol formation. The exact mechanism of such a process should it exist is not known.

The stability of a complex of SO_2 and H_2O was first suggested by Phillips from results of semiempirical calculations (Ref. 19). Holland and Castleman using CNDO/2 calculations suggested that an $\text{SO}_2 \cdot \text{H}_2\text{O}$ adduct should be stable in the gas phase and reported a binding energy of 145 mH and a large dipole moment (Ref. 20).

Evidence for the existence of $\text{H}_2\text{O} \cdot \text{SO}_2$ produced from the photolysis of H_2S in solid O_2 at 15K by ultraviolet light is presented by Tso and Lee who conducted an FTIR study of the photolysis mixture (Ref. 21). Identification was based on shifted vibrational bands of SO_2 and H_2O .

The stability of SO_2 -water complexes has also been suggested from molecular beam measurements, and electric deflection experiments indicate a large dipole moment for the complex (Ref. 22).

Although there have been no ab initio calculations of the $\text{SO}_2 \cdot \text{H}_2\text{O}$ complex there are calculations for related complexes. Ab initio calculations on $\text{SO}_2 \cdot \text{NH}_3$ (Ref. 23) and $\text{SO}_2 \cdot \text{HF}$ (Ref. 24) show stable complexes for a variety of geometries.

An important pair of calculations were done on the closely related complex $\text{H}_2\text{O}\cdot\text{SO}_3$ and its rearrangement to H_2SO_4 . A semiempirical CNDO/2 calculation by Holland and Castleman (Ref. 25) has been followed by a recent ab initio calculation by Chen and Plummer (Ref. 26).

In an effort to shed some light on a possible role of H_2O in the oxidation of SO_2 and elucidate the structure and energetics of formation of water complexes of SO_2 , we have undertaken an ab initio study.

The study began with a reasonably sophisticated SCF-CI treatment of two geometries of the $\text{H}_2\text{O}\cdot\text{SO}_2$ complex. These are I and II in Fig. 11. The geometries of the fragments were frozen at the minimum energy theoretical geometries. The values used are: H_2O ($R_{\text{OH}} = 0.956\text{\AA}$, $\angle_{\text{HOH}} = 105.2^\circ$) and SO_2 ($R_{\text{SO}} = 1.423\text{\AA}$, $\angle_{\text{OSO}} = 118.4^\circ$). The generally contracted (Ref. 27) basis sets used were: H_2O (9s5p/5s)/<3s2p/2s> and SO_2 (12s9p/9s5p)/<4s3p/3s2p>. Van Duijneveldt exponents (Ref. 14) were used for H and O orbitals while the exponents for S were from Huzinaga (Ref. 28).

The potential energy surface was studied at the SCF level. A configuration interaction (CI) treatment was performed at the energy minimum of each conformation. Two different frozen cores were used and all single and double excitations outside the frozen core virtual orbitals were included. In CI1 the frozen core included the 2s orbital of oxygen and the 3s orbital of sulfur as well as the inner shell orbitals of sulfur and oxygen. This restriction generated 2653 configurations and 4453 cfs. In CI2 the frozen core included just the inner shell orbitals of sulfur and oxygen and generated 5547 configurations and 9735 cfs. The selection criterion in both cases was a cumulative discard of terms less than 5×10^{-5} a.u.

The SCF potential energy surface showed a gradual slow decrease in the total energy as the interfragment distance was reduced, reaching a shallow minimum for the two conformations, then rising steeply to become repulsive at distances only 0.6\AA less than that which gave the minimum total energy. The most stable distance of conformation I was 6.1 a.u. while for conformation II the energy minimum was reached at $R = 5.5$ au and $r = 1.6$ au with the $S(SO_2)$ to $O(H_2O)$ distance equal to 5.73 au.

The binding energies of conformations I and II are shown in Table 17 for the two CI approaches. Conformation II is clearly bound for all approaches while conformation I becomes unbound for the CI2 approach which substantially reduces the binding energy for both conformations over that of CI1.

The results of a Mulliken population analysis (Ref. 29) are shown in Table 18. The SCF results for conformation II show a large movement of charge relative to the SCF results of the separated fragments while the corresponding results for conformation I show no large changes. The CI2 approach reduced the intermolecular charge transfer of conformation II to 0.001 electron. The intramolecular charge movement is also very small.

Two basis set concerns were addressed as a part of these early calculations. Polarization functions (3d on sulfur, 2p on hydrogen) were added to the basis set. The augmented basis set decreased the binding energy by 2mH for the particular test geometry chosen. The effect of basis set superposition at the SCF level was found by using ghost orbitals in place of one of the fragments positioned at the minimum energy interfragment distance. The total energy was compared with a similar calculation for $R = 100$ au. The energy difference was 1.2 mH indicating only a small superposition error at the SCF level with the basis set used.

To explore the possibility of other metastable conformations of $\text{H}_2\text{O}\cdot\text{SO}_2$ an SCF energy gradient program (Ref. 30) was used to locate stable structures for the complexes. The 4-31G basis set available in the gradient package was used for the potential energy searches.

Five distinct conformations of the single water complex $\text{H}_2\text{O}\cdot\text{SO}_2$ were found to be bound. These are shown in Fig. 12 together with some of the minimum energy geometry information. The total energies for the complexes and the molecular fragments as well as the binding energies are given in Table 19.

For conformation I the geometry is almost exactly the same as it was with the earlier calculation with the larger basis set and the binding energy is slightly greater by 1.5 mH. For conformation II the complex is found to be a little more compact and the binding energy is 2.6 mH greater than with the larger basis set. It should be noted that the gradient calculation did not freeze the geometries of the fragments. Conformation II should be viewed as a nascent sulfurous acid molecule (H_2SO_3) since a hydrogen transfer and subsequent redistribution of electrons would give $\begin{array}{c} \text{O} \\ \parallel \\ \text{HOSO} \end{array}$ the presumed structure of sulfurous acid.

Conformations III and IV represent single and double hydrogen-bonded structures, respectively. In conformation III the out-of-plane angle of rotation of the nonhydrogen-bonded OH is very soft energetically and no angle is favored energetically by more than a few tenths of a milliHartree. Conformation V was suggested by the results of a semiempirical calculation (Ref. 20), but the minimum energy geometry result here indicates a preference for a cis arrangement rather than the trans arrangement of the semiempirical calculation.

Two-water complexes were studied using the energy gradient program with the 4-31G basis set. The conformations are shown in Fig. 13. Conformations VI and VII are mirror image doublings of conformations II and V, respectively. The interatomic distance did not change significantly in going to the two-water complexes. The energies are given in Table 19. In both cases the binding energies of the two-water complexes are a little less than twice the binding energies of the one-water complexes indicating relatively little interaction between the water molecules and almost independent addition of the second water molecule.

To examine the effect of basis set size on the binding energy and geometry two additional SCF energy gradient calculations were performed on conformation V. In the first calculation a double zeta basis set with McLean exponents was employed (Ref. 31). The binding energy decreased by 3mH, a rough measure of the superposition error in the poorer basis set. In the second calculation a set of sulfur 3d orbitals ($\alpha = 0.6$) was added to the double zeta basis set. The polarization functions reduced the SO_2 bond angle, decreased the SO_2 dipole moment, and lowered the binding energy of the complex by 2.4 mH. The results of these two calculations are given in Table 19.

In order to examine the energetics of adding multiple waters to SO_2 and still retain the double zeta plus sulfur d orbital basis set, SCF calculations were run using a generally contracted basis set at fixed geometries predicted by the earlier gradient results. The primitive basis set was a Huzinaga sulfur (12s/8p) oxygen (9s/5p), hydrogen (4s) set generally contracted to $\langle 4s/3p \rangle$, $\langle 3s/2p \rangle$, and $\langle 2s \rangle$, respectively, (Refs. 7,28). This set was augmented by a single set of 3d functions ($\alpha = 0.6$) on the sulfur atom. This basis set was similar to the previous

double zeta plus d set and the binding energy of conformation V obtained with this new basis set differed by only 0.2 mH from the previous result.

The multiple-water complexes studied are shown in Fig. 13. The total energies and binding energies are given in Table 19. Conformation I with this basis set produces a binding energy which is 72% of the binding energy derived from the earlier 4-31G calculation. This reduction in binding energy is virtually identical to that obtained for conformation V. The two-, three-, and four-water complexes differ by only a few mH from the sum of the binding energies of the separate bound pairs. This assumes that the energies of the conformations II and IV (which were not run with the new basis) can be approximated by taking 70% of the binding energy obtained with the 4-31G basis set. The binding energy of the five-water complex is, however, significantly less than the sum of the binding energies of the separate bound-pairs.

The implications of the additivity of the binding energies supports the notion that the bonding interaction is nearly purely electrostatic. Only when the waters were close enough to interact with each other, as in the five-water complex, did the binding energy fall significantly below the sum of the binding energies of the separate bound pairs. An interesting corollary to the approximate additivity of the binding energies occurred in the three-water complex which was slightly more stable than predicted from the binding energy additivities perhaps due to a favorable alignment of the water dipoles.

Although a Morakuma component analysis (Ref. 32) of the energy components of the $\text{H}_2\text{O} - \text{SO}_2$ interaction was not made, the results obtained here suggest that the analysis would follow that for the $\text{NH}_3 \cdot \text{SO}_2$ complex (Ref. 23) as discussed by Kollman (Ref. 33). The charge transfer and

polarization affects are small and the minimum energy geometry is determined by a balance of the electrostatic energy and the exchange repulsion energy. However, unlike the $\text{NH}_3 \cdot \text{SO}_2$ complex, the minimum energy geometry for the $\text{H}_2\text{O} \cdot \text{SO}_2$ complex (conformation V) is close to that predicted solely from consideration of dipole-dipole interaction.

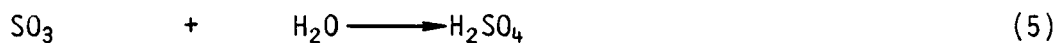
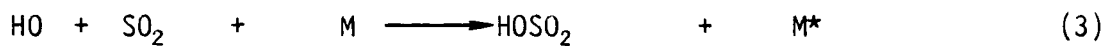
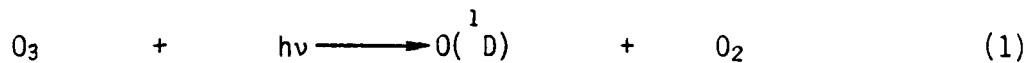
The H-bonded complex (conformation III) has a binding energy ($7.5 \text{ mH} = 4.7 \text{ Kcal}$) which is virtually the same as that obtained for the $\text{HF} \cdot \text{SO}_2$ complex (5 Kcal) (Ref. 24). The minimum energy geometry complex (conformation V) has a binding energy ($17.4 \text{ mH} = 10.9 \text{ Kcal}$) very close to that obtained for the $\text{NH}_3 \cdot \text{SO}_2$ complex (9.3 Kcal) (Ref. 23). It should be noted that inclusion of d orbitals in the sulfur basis set reduced the binding energy ($10.4 \text{ Kcal} \rightarrow 9.3 \text{ Kcal}$) of $\text{NH}_3 \cdot \text{SO}_2$, an effect that was observed in the $\text{H}_2\text{O} \cdot \text{SO}_2$ calculations. The CNDO/2 results of Castleman gave a much larger binding energy ($145.9 \text{ mH} = 98.3 \text{ Kcal}$) and a different minimum energy geometry (Ref. 20).

In the analysis of his molecular beam electric deflection results Castleman remarks on the existence of species with large dipole moments that he attributes to $\text{H}_2\text{O} \cdot \text{SO}_2$ complexes (Ref. 22). The dipole moments for some of the complexes were calculated in this study and are reported in Table 20. These values are all overestimated particularly those from calculations not using sulfur d orbitals.

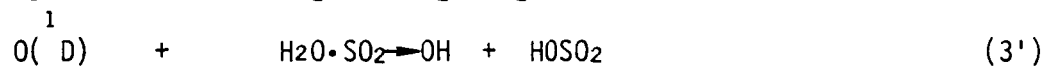
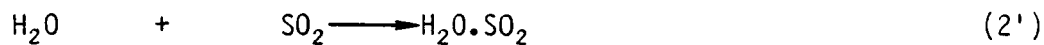
The geometry optimization routine also produced force constants and fundamental frequencies for vibrational modes. However, the results did not converge to sufficient accuracy to predict the sizes and signs of the frequency shifts of SO_2 and H_2O vibrations upon complexation. Better convergence would allow comparison with the experimental IR spectroscopic results of Tso and Lee who claim to have evidence for the existence of the

H₂O·SO₂ complex (Ref. 21).

There are two implications from these results for acid rain chemistry. The most widely accepted mechanism for the tropospheric, gas phase production of H₂SO₄ is as follows:



This ab initio study shows that an H₂O·SO₂ complex is predicted to be stable and therefore an alternative to steps (2) and (3) above is suggested:



where the complex could act as its own energy sink negating the need for a third body. A comparison of the activation energies for the alternatives is needed to decide between them.

The second implication for acid rain chemistry comes from the results of the multiple-water complexes. There appears to be a shell of bonding sites for H₂O around a central SO₂. This suggests the formation of a nucleation center with additional waters outside the initial sphere added in a typical H-bonded fashion to waters already in the complex. The energetics are favorable but a discussion of the position of equilibrium would have to include an evaluation of the entropy changes for the process. The formation of an SO₂-containing droplet would allow heterogeneous chemistry to proceed.

In summary an energy gradient program was used to locate stable structures for $\text{H}_2\text{O}\cdot\text{SO}_2$ complexes and SCF calculations were carried out to determine the binding energies of complexes with multiple water molecules. A 4-31G basis set was used for most potential energy searches. More accurate basis sets including a generally contracted basis set with d orbitals on the sulfur atom were used for geometry and binding energy verification. For one water complexes five different stable geometries were located, with binding energies between 4 and 11 Kcal mol⁻¹ suggesting a binding shell for H_2O around SO_2 . Very little charge transfer between SO_2 and H_2O was present. Addition of more than one H_2O was found to be energetically favorable and approximately additive up to four added waters. An alternative mechanism for the tropospheric, gas phase production of acid rain is suggested which does not require a third body. A process for the formation of an SO_2 -containing water droplet is advanced.

Table 17. Total energies (Hartrees) and binding energies (milliHartrees in parentheses) of conformations I and II and the separated fragments showing the effects of configuration interaction.

	SCF	CI1	CI2
Separated fragments	-622.9726	-623.1224	-623.1793
Conformation I	-622.9786 (-6.0)	-623.1339 (-11.25)	-623.1539 (+25.4)
Conformation II	-622.9824 (-9.8)	-623.1457 (-23.3)	-623.1918 (-12.5)

Table 18. Mulliken population analysis of conformations I and II and separated fragments showing effect of configuration interaction.

	Atom	SCF	CI2
Separated fragments	S	+1.20	+1.16
	O ₁	-0.60	-0.58
	O ₃	-0.72	-0.71
	H	+0.36	+0.355
Conformation I	S	+1.23	
	O ₁	-0.62	
	O ₃	-0.74	
	H	+0.37	
	charge transfer	0.004 → SO ₂	
Conformation II	S	+2.35	+1.20
	O ₁	-2.12	-0.60
	O ₂	-0.75	-0.61
	O ₃	-0.23	-0.74
	H ₁	+0.37	+0.37
	H ₂	+0.38	+0.38
		charge transfer	0.52 → SO ₂

Table 19. SCF total energies (Hartrees) and binding energies (milliHartrees in parentheses) of $\text{SO}_2 \cdot (\text{H}_2\text{O})_n$ complexes.

	Geometry Optimized			Geometry fixed
H ₂ O	-75.9086	-76.0110	-76.0110	-76.012 ¹
SO ₂	-546.3733	-546.9719	-547.1540	-547.1755
I	-622.2894(7.5)	-	-	-623.1930(5.4)
II	-622.2943(12.4)	-	-	-
III	-622.2894(7.5)	-	-	-
IV	-622.2902(8.3)	-	-	-
V	-622.2993(17.4)	-622.9973(14.4)	-623.1770(12.0)	-623.1998(12.2)
VI	-698.2120(21.5)	-	-	-
VII	-698.2236(33.1)	-	-	-699.2212(21.5)
VIII	-	-	-	-775.2437(31.9)
IX	-	-	-	-851.2560(32.1)
X	-	-	-	-927.2703(34.3)
Basis Set	A	B	C	D

A: 4.31G

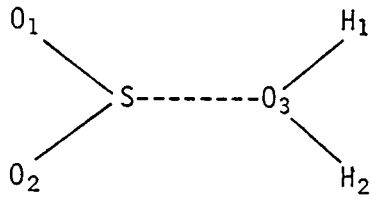
B: Double Zeta

C: Double Zeta + Sulfur d

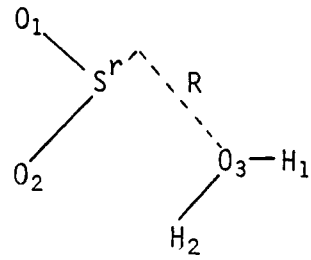
D: S(12s/8p)/<4s/3p7, 0(9s/5p)/<3s/2p>, H(4s)/<2s>

Table 20. Dipole moments (in Debyes) for fragments and selected complexes from SCF geometry optimizations.

H ₂ O	2.49	2.53	2.53
SO ₂	-	3.44	2.67
III	6.10	-	-
IV	6.35	-	-
V	2.95	2.92	2.51
Basis set	A	B	C



I



II

Figure 11. Conformations of $\text{SO}_2 \cdot \text{H}_2\text{O}$ complexes.

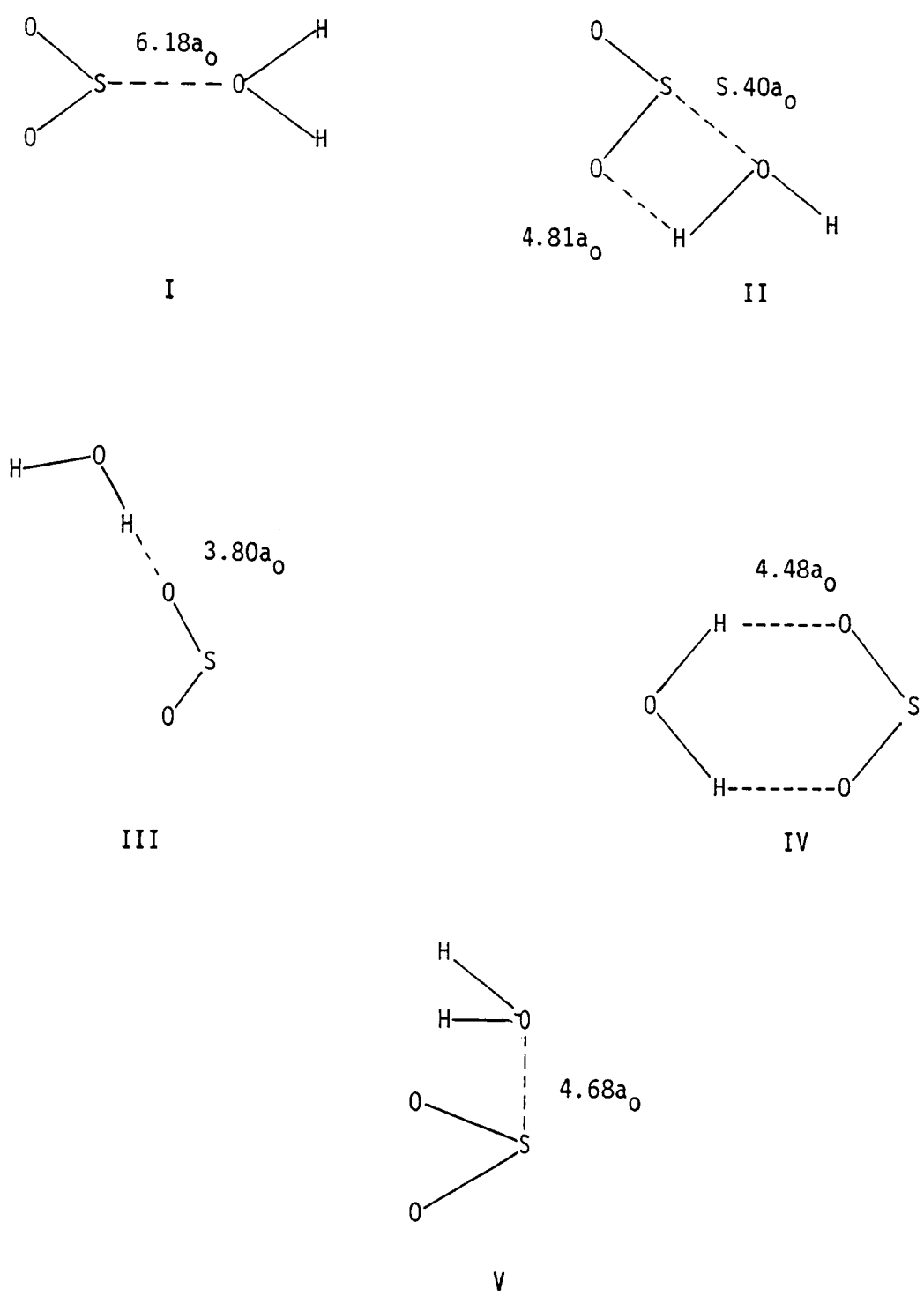
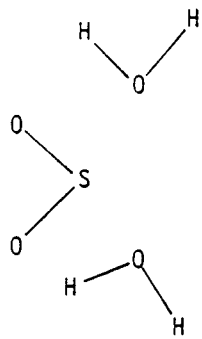
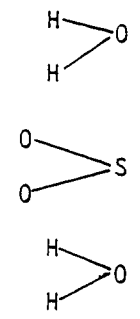


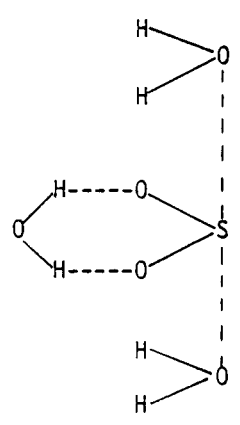
Figure 12. Conformations of $\text{SO}_2 \cdot \text{H}_2\text{O}$ complexes including some minimum energy geometry results.



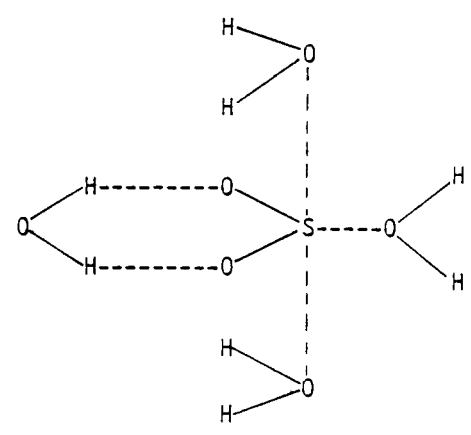
VI



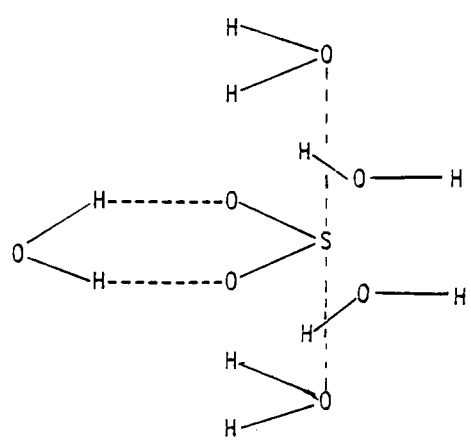
VII



VIII



IX



X

Figure 13. Conformations of multiple-water complexes of SO_2 .

ADDENDUM

Other projects under study during the grant period included some work on computational technique to study the above described systems. The most significant of these was the development and implementation of a method to calculate transition moments between non-orthogonal molecular orbitals by the use of corresponding orbitals. The details of the theory with some application have been published and a reprint of the article is attached with this report. A theoretical method was implemented to compute the vibrational frequencies, the overlaps between vibrational functions in a given electronic state and to determine the vibrational transition moments between various states.

Other efforts included interfacing the BIGMOLI system of programs with SCF and CI programs modified by other researchers at the Langley Research Center. Also the energy gradient integral program package received from the Quantum Chemistry Program Exchange was implemented at the Langley Research Center Computer Complex.

Initial calculations on the triplet state potential energy surface



were carried out using the energy gradient integral program package. The aim of these calculations was to study the stability and energetics of HO_2OH complex. These calculations were postponed until the MCSCF procedure has been incorporated into the energy gradient integral program package. Investigations of the lowest singlet state chemically bonded and hydrogen bonded intermediates in this reaction have been pursued in other efforts at the Langley Research Center.

ACKNOWLEDGMENTS

The research described in this Final Report was supported by the NASA Langley Research Center under NASA Grant NSG 1393. The project was monitored by Donald H. Phillips, NASA/Langley Instrument Research Division.

REFERENCES

1. J. N. Pitts, Jr., NASA Ref. Publication 1022, p. 53 (1978).
2. C. L. Shaw, Ibid pp. 65-79.
3. D. A. Parkers, D. M. Paul, C. P. Quinn, and R. C. Robson, Chem. Phys. Lett. 23, 425 (1973).
4. R. A. Bair, and W. A. Goddard III, J. Am. Chem. Soc. 104, 2719 (1982).
5. W. J. Hunt, P. J. Hay, and W. A. Goddard III, J. Chem. Phys. 57, 738, (1972); Babrowicz, F. W., and Goddard III, W. A. in Modern Theoretical Chemistry edited by H. F. Schaefer, III. (Plenum Press, N. Y. 1977), Vol III, p. 189.
6. T. M. Dunning, Jr., J. Chem. Phys. 53, 2823 (1970).
7. S. Huzinaga, J. Chem. Phys. 42, 1293 (1965).
8. GVB program written by Hunt, May and Goddard III, J. Chem. Phys. 57, 738 (1972) extensively modified by Bauschlicher and Lengsfeld at Langley Research Center, which avoids extensive I/O requirements for uses with several GVB programs and has several convergence options.
9. I. Shavitt in Modern Theoretical Chemistry, edited by H. F. Schaefer III, (Plenum Press, N. Y. 1977) Vol III, p. 189 and references therein.
10. A. Arkell, R. Reinhard and L. P. Lesson, J. A. Chem. Soc. 87, 1016 (1965); A. Arkell, J. Chem. Phys. 73, 3877 (1969).
11. L. Andreas, J. Chem. Phys. 57, 51 (1972).
12. P.A. G. O'Hare and A. C. Wahl, J. Chem. Phys. 53, 2469 (1970).
13. W. A. Latham, L. A. Curtiss, W. J. Mehr, J. B. Liske and J. A. Pople. Proj. Org. Chem. 11, 175 (1974).
14. F. B. Van Duijneveldt, IBM Research Report RJ 945 (16437) December 10, 1971.
15. B. M. Lengsfeld III, J. Chem. Phys. 73, 382 (1980).
16. S. R. Langhoff, C. W. Bauschlicher, Jr. and M. Partridge, Chem. Phys. Lett. 102, 292 (1983).
17. J. G. Calvert, A. Lazrus, G. L. Kok, B. G. Heikes, J. G. Walega, J. Lind, and C. A. Cantrell, Nature 317, 27 (1985).
18. R. H. Heist and H. Reiss, J. Chem. Phys. 11, 573 (1974).
19. D. H. Phillips, Bull. Am. Phys. Soc., Ser. 2, 19, 237 (1974).

20. P. M. Holland and A. W. Castleman, Jr., J. Photochem. 16, 347 (1981).
21. T. L. Tso and E. K. C. Lee, J. Phys. Chem. 88, 2776 (1984).
22. A. W. Castleman, Jr., in "Heterogeneous Atmospheric Chemistry," p. 13-27, D. R. Schryer, Ed., American Geophysical Union, Washington, DC, 1982.
23. R. R. Lucchese, K. Haber, and H. F. Schaefer III, J. Am. Chem. Soc. 98, 7617 (1976).
24. M. F. Friedlander, J. M. Howell, and A. M. Sapse, Inorg. Chem. 22, 100 (1983).
25. P. M. Holland and A. W. Castleman, Jr., Chem. Phys. Lett. 56, 511 (1978).
26. T. S. Chen and P. L. Moore Plummer, J. Phys. Chem. 89, 3689 (1985).
27. R. C. Raffenetti, J. Chem. Phys. 58, 4452 (1973).
28. S. Huzinaga, "Approximate Atomic Functions II," Dept. of Chem. Report, Univ. of Alberta, Edmonton, Alberta, Canada, 1971.
29. R. S. Mulliken, J. Chem. Phys. 23, 1833 (1955).
30. (a) J. W. McIver, Jr. and A. Kormornicki, Chem. Phys. Lett. 10, 303 (1971); (b) A. Kormornicki, K. Ishida, K. Morokuma, R. Ditchfield, and M. Conrad, *ibid.* 45, 595 (1977).
31. A. D. McLean and G. S. Chandler, IBM Research Report RJ2665 (34180), October 15, 1979.
32. K. Morokuma, J. Chem. Phys. 55, 1236 (1971).
33. P. Kollman, J. Am. Chem. Soc. 99, 4875 (1977).

APPENDIX

The lower electronic states of ClOO: A computational investigation

Jawed A. Jafri

Old Dominion University Research Foundation, Mail Stop 234, NASA-Langley Research Center, Hampton, Virginia 23665

Byron H. Lengsfeld, III^{a)}

Laser and Spectroscopy Branch, NASA-Langley Research Center, Hampton, Virginia 23665

Charles W. Bauschlicher, Jr.^{b)}

Institute for Computer Applications in Science and Engineering, Langley Research Center, Hampton, Virginia 23665

Donald H. Phillips

General Research Instrumentation Branch, Mail Stop 234, NASA-Langley Research Center, Hampton, Virginia 23665

(Received 3 May 1984; accepted 7 May 1985)

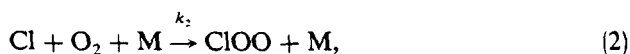
Eight doublet and eight quartet states of ClOO were investigated by *ab initio* CI techniques. The potential energy surfaces of the four lowest energy doublet states of both A'' and A' symmetry indicate that only the $1^2A''$ state is bound. In contrast to the model provided by the HO₂ radical, all of the excited doublet states investigated were repulsive with respect to dissociation to Cl + O₂ and metastable or bound with respect to dissociation to ClO + O. The transitions to the excited states investigated span the visible and near UV spectral regions, but the transition moments indicate that they are very weak. Since the photolysis products are the same as those of the rapid thermal dissociation, photolysis is not expected to be an important atmospheric process. The soft bending potential for the $1^2A'$ state and the shape of the $1^4A''$ state in the entrance channel of the ClO + O → Cl + O₂ reaction provide a qualitative explanation for the underprediction of the low temperature reaction rate by previous trajectory calculations.

I. INTRODUCTION

Destruction of stratospheric ozone by reaction (1),



is accompanied by the side reactions



and



The ratio of the rates of (1) and (2) and of the concentration of ozone to that of molecular oxygen are such that reactions (1) and (2) occur at approximately equal rates in the upper atmosphere where ozone destruction by chlorine from anthropogenic sources is an important concern. Reaction (3) is not considered a major factor in the atmosphere, but may be important in laboratory investigations of the chemistry of ozone and chlorine.¹ In spite of its high rate of formation by reaction (2) the ClOO molecule is not considered very important in atmospheric chemistry because it rapidly dissociates by the reverse reaction. If the ClOO radical undergoes rapid reactions, however, these additional reactions could be important to the atmospheric chemistry of chlorine and/or other trace species. A reaction involving the oxidation of

another atmospheric species, such as the oxidation of CO by ClOO proposed by Prinn² to explain the CO/CO₂ ratio on Venus, could play a role; but no rapid reaction of that type has been observed. Photolysis is another reaction which, depending upon the active wavelengths and products, could be important. Johnston, Morris, and Van den Bogaerde³ observed a portion of the ultraviolet spectrum of ClOO by the use of modulation spectroscopy, but did not determine the products. In addition, Eachus *et al.*^{4(a)} tentatively assigned an absorption feature observed at 380 nm in the photolysis products of ClO₂ (in H₂O/H₂SO₄ matrices at 77 K and in crystalline KClO₄) to the ClOO radical. The production of O(¹D) is energetically possible at the wavelengths of Johnston *et al.*'s observations and O(³P) could be produced at longer wavelengths, which would not be subject to screening by ozone absorption in the atmosphere. Eachus *et al.*^{4(a)} observed thermal isomerization of the ClOO radical to the symmetric ClO₂. Photoisomerization from ClOO to OClO could also be significant, but only the reverse process was observed in Arkell and Schwager's^{4(b)} matrix isolation investigations of the infrared spectrum of ClOO. Other experimental investigations of ClOO have provided information on its heat of formation and rates of formation and dissociation.⁵ In a theoretical study, Gole and Hayes⁶ evaluated the energy of ClOO relative to that of OClO. They used the restricted SCF method for OClO and ClOO⁻, but had to use the orbitals of the latter calculation for neutral ClOO because of convergence difficulties.

The present investigation is focused on providing further information on the photolysis spectrum and pro-

^{a)}National Research Council Associate. Present address: Ballistics Research Laboratory, ORDAR-BLL, Aberdeen, MD 21005.

^{b)}Present address: NASA-Ames Research Center, STS 230-3, Moffett Field, CA 94035.

ducts:



in order to provide for an assessment of the atmospheric importance of this process. Information on the lower states of ClOO is also of interest with regard to the reaction



which is an important element of the catalytic cycle for ozone destruction. A theoretical investigation⁷ of this reaction relied on several assumptions regarding the lower states of ClOO and apparently underestimated the reaction rate. Recent experimental investigations⁸ obtained approximately the same rate at 298 K, but gave significantly different temperature dependencies. The results from the investigation of the states of ClOO, which is an intermediate in Eq. (5), will be useful for understanding this reaction and the underprediction of the rate by the trajectory calculations.

Finally, understanding the electronic states of ClOO will provide a model in addition to that of HO₂, for understanding the range of photochemical behavior to be expected of peroxy compounds. Specifically, the states of FOO which may be of significance in atmospheric fluorine chemistry should be closely related to those of ClOO. The size of the ClOO molecule, the number of electronic states of interest, and the nature of its photochemical properties make this problem a significant computational task. The methods used to accomplish this task are discussed in the following section. The results obtained are presented and discussed in subsequent sections.

II. COMPUTATIONAL METHODS

A. Basis sets

The (9s5p) Cartesian Gaussian basis of van Duijneveldt⁹ for oxygen and the (12s9p) set of Huzinaga¹⁰ for chlorine were generally contracted¹¹ to (3s2p) and (4s3p), respectively, and augmented by a set of *s* and *p* bond centered functions¹² to provide for polarization. The exponents of the bond function were 0.7 (*s*) and 0.6 (*p*).

The molecular orbitals were taken from a limited "pairs only" MCSCF treatment of the X^2A'' ground state in which the SCF configuration (CSF)

$$\psi_{\text{SCF}} = \dots (10a')^2 (11a')^2 (12a')^2 (13a')^2 (2a'')^2 (3a'')^2 4a''$$

was augmented by CSF's in which the $\sigma(\text{O}-\text{O})$ and $\sigma(\text{Cl}-\text{O})$ bonding orbitals were replaced by their respective antibonding orbitals. Examination of CI treatments utilizing orbitals from more extensive pairs only MCSCF treatments and from MCSCF treatments of the $1^2A'$ state indicated that the above choice is superior. In the SCF description of the X^2A'' state, the $10a'$ orbital is a lone pair on the terminal oxygen, $11a'$ is the O-O bonding orbital, $12a'$ is the Cl lone pair orbital and $13a'$ is the Cl-O bonding orbital. The out-of-plane orbitals $2a''$, $3a''$, and $4a''$ are somewhat localized on Cl, the central O atom, and the terminal O atom, respectively.

Preliminary configuration interaction (CI) calculations indicated that all of the configurations of importance arise from rearrangements of the electrons within the occupied

orbitals and excitations to the $14a'$ and $15a'$ orbitals which are the Cl-O and O-O antibonding orbitals, respectively. The results of these calculations further indicated that excitations from the molecular orbitals arising from core orbitals and pseudo core orbitals arising primarily from the Cl (3*P*) and O (2*S*) components were not important to any of the states of interest. Although the most important CSF's for describing the lower states of either symmetry were the same at widely varying points on the potential energy surfaces, a relatively larger number of CSF's were of minor importance at some points on the surface. At a given point on the potential energy surfaces between 20 and 50 CSF's made at least a 1% contribution to one of the four lowest doublet states. Supplementary calculations on the effect of varying the reference list across the surface indicated that only minor "noise" would result. This is in agreement with recently published investigations.¹³ The reference CSF's actually used at each geometry were selected from "frozen core" full valence CI calculations on the lowest four roots of each symmetry.

A list of target CSF's was generated by including all single and double excitations from the reference list subject to the restrictions (1) that the true core orbitals remain fully occupied, (2) that only one hole could exist in the orbital space arising from the chlorine 3*P* and oxygen 2*S* atomic orbitals, and (3) that only one electron could occupy the external (nonvalence) portion of the orbital space.

A final CSF list was prepared by selecting CSF's from the target list according to their A_k contributions^{13(b)} to the first four roots using a cumulative threshold of 60 mhartree. In most calculations all single excitations with respect to the most important CSF for each of the four states of interest were retained without regard for their energy contributions.

The perturbation theory estimates of the energy contributions, to each root, for all rejected CSF's were added to the raw eigenvalues in order to obtain comparable energies for the different states and for the same state at different geometries. Extensive calculations were carried out using smaller thresholds to determine the extent of the potential energy surface noise introduced by the selection and energy adjustment procedures. The effect of selection threshold on the convergence of dipole moments and transition moments was also investigated. The potential energy noise was found to be about 10% of the cumulative threshold in amplitude. This agreed with earlier unpublished results.¹⁴ Although the computed dipole moments and transition moments were quite small, the results obtained using the procedures discussed above led to values which were converged to within 40% of the values obtained using small thresholds. The overall results of the calculations which were carried out to assess the accuracy of the present methods was to insure that the results would provide sufficient accuracy for the major goals of this study. In addition to the above CI calculations, a few additional calculations were carried out on the X^2A'' ground state using a smaller (5 mhartree) threshold and natural orbitals obtained from the above calculations. The reference wave function for the natural orbital calculations included all CSF's which contributed 0.25% or more to a (frozen core) full valence CI wave function. The target CSF list for the natural orbital CI was formed using the prescription de-

TABLE I. Energies of ${}^2A''$ and ${}^2A'$ states.^a

Calc#	R (ClO)	R (OO)	ClOO	$1^2A''$	$2^2A''$	$3^2A''$	$4^2A''$	$1^2A'$	$2^2A'$	$3^2A'$	$4^2A'$
1	3.6	2.0	113.6	-0.2019	-0.0828	-0.0633	-0.0405	-0.1251	-0.0867	-0.0498	-0.0393
2	3.6	2.2	113.6	-0.2711	-0.1585	-0.1379	-0.1285	-0.1917	-0.1706	-0.1244	-0.1242
3	3.6	2.48	113.6	-0.2881	-0.1808	-0.1693	-0.1489	-0.2211	-0.2077	-0.1563	-0.1489
4	3.6	2.6	113.6	-0.2809	-0.1762	-0.1668	-0.1494				
5	3.6	2.8	113.6	-0.2636	-0.1689	-0.1420	-0.1336	-0.2247	-0.1833	-0.1344	-0.1352
6	3.6	3.1	113.6	-0.2378	-0.1600	-0.1308	-0.0966	-0.2157	-0.1628	-0.1237	-0.1078
7	3.6	3.5	113.6	-0.2008	-0.1415	-0.1398	-0.1299	-0.1927	-0.1542	-0.1324	-0.0801
8 ^b	3.6	4.2	113.6 ^b	-0.1713	-0.1538	-0.1509	-0.0816	-0.1817	-0.1621	-0.1452	-0.1157
9 ^b	3.6	5.0	113.6 ^b	-0.1605	-0.1596	-0.1566	-0.0802	-0.1631	-0.1617	-0.1593	-0.0789
10	3.1	2.48	113.6	-0.2717	-0.1134	-0.0648	-0.0254				
11	3.3	2.48	113.6	-0.2807	-0.1485	-0.1185	-0.0948	-0.2192	-0.1657	-0.1134	-0.0929
12	3.45	2.48	113.6	-0.2848	-0.1642	-0.1485	-0.1462				
13	3.75	2.48	113.6	-0.2881	-0.1969	-0.1815	-0.1776	-0.2219	-0.1973	-0.1684	-0.1657
14	3.90	2.48	113.6	-0.2878	-0.2124	-0.2048	-0.1900	-0.2303	-0.2160	-0.1939	-0.1800
15	4.3	2.48	113.6	-0.2910	-0.2423	-0.2355	-0.2902				
16 ^b	5.0	2.48	113.6 ^b	-0.2862	-0.2718	-0.2458	-0.2358	-0.2470	-0.2450	-0.2334	-0.2115
17 ^b	7.0	2.48	113.6	-0.2829	-0.2794	-0.2449	-0.2338				
18 ^b	25.0	2.40	180.0	-0.2816	-0.2809	-0.2408	-0.2383				
19	3.75	2.48	80.0	-0.2206	-0.1943	-0.1732	-0.1214	-0.2019	-0.1639	-0.1342	-0.1255
20	3.75	2.48	95.0	-0.2704	-0.2004	-0.1792	-0.1560	-0.2232	-0.1928	-0.1642	-0.1478
21	3.75	2.48	105.0	-0.2847	-0.1989	-0.1808	-0.1736	-0.2277	-0.2099	-0.1706	-0.1602
22	3.75	2.6	113.6	-0.2803	-0.1914	-0.1805	-0.1707				
23	3.75	2.48	122.0	-0.2863	-0.1977	-0.1782	-0.1763	-0.2259	-0.2111	-0.1722	-0.1712
24	3.75	2.48	140.0	-0.2722	-0.2010	-0.1835	-0.1692	-0.2188	-0.2028	-0.1711	-0.1646
25	3.75	2.48	160.0	-0.2493	-0.2076	-0.1880	-0.1593	-0.2131	-0.1919	-0.1730	-0.1506
26	3.75	2.48	180.0	-0.2221	-0.1912	-0.1711	-0.1090	-0.2070	-0.1961	-0.1807	-0.1562
27	3.75	2.3	180.0	-0.2335	-0.2016	-0.1961	-0.1458				
28	3.75	2.8	180.0	-0.2018	-0.1858	-0.1738	-0.1381				
29	3.75	2.1	160.0	-0.2110	-0.1616	-0.1445	-0.1060				
30	3.75	2.3	160.0	-0.2464	-0.2021	-0.1849	-0.1464				
31	3.75	2.8	160.0	-0.2126	-0.1742	-0.1454	-0.1364				
32	3.75	3.1	160.0	-0.1827	-0.1494	-0.1421	-0.1177				
33	3.75	2.36	113.6	-0.2906	-0.1968	-0.1819	-0.1721				
34	3.2	3.5	113.6	-0.2194	-0.1560	-0.1477	-0.1362				
35	3.4	3.5	113.6	-0.2161	-0.1497	-0.1438	-0.1267				
36	3.3	2.3	113.6	-0.2710	-0.1237	-0.1078	-0.0817				
37	3.3	2.6	113.6	-0.2781	-0.1282	-0.0957	-0.0683				
38	3.6	2.48	105.0	-0.2832	-0.1800	-0.1663	-0.1504				
39	4.1	2.48	113.6	-0.2891	-0.2279	-0.2260	-0.2035				
40	4.5	2.48	113.6	-0.2896	-0.2549	-0.2399	-0.2190				

^a Energies in hartrees relative to -609.0 hartree. Although energies are given to four decimal places the uncertainty introduced by the selection and extrapolation procedure occurs in the third decimal place (see the text).

^b Forced retention of single excitation was not used in these calculations.

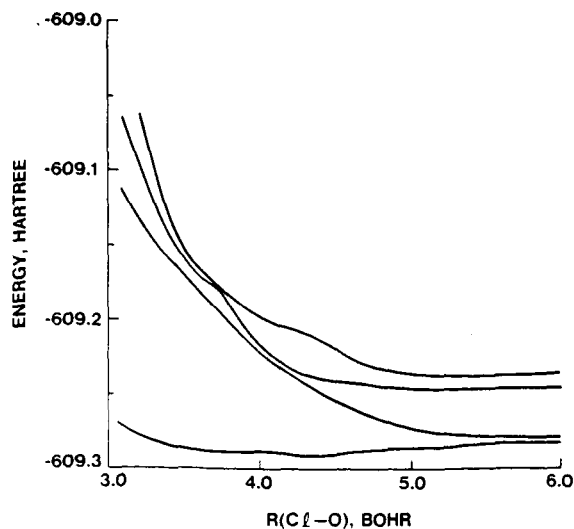


FIG. 1. CI energies of ${}^2A''$ states as a function of R (ClO). The ClOO angle is constant at 113.6 deg and R (OO) equals 2.48 bohr.

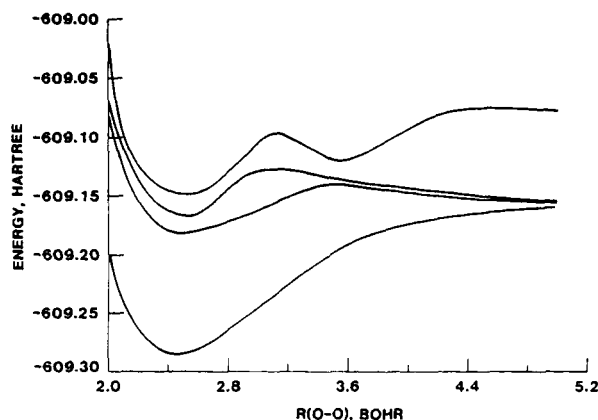


FIG. 2. CI energies of the ${}^2A''$ states as a function of R (OO). The ClOO angle is 113.6 deg and R (ClO) is 3.6 Bohr.

scribed above.

III. RESULTS

The energies obtained for the eight doublet states treated are presented in Table I for each of the geometries investigated. The natures of the potential energy surfaces are discussed below. Some of the data from Table I is duplicated in figures for the sake of clarity.

A. The ${}^2A''$ states

Slices through the potential energy surfaces of the four lowest ${}^2A''$ states along the ClO and OO bond stretching coordinates are shown in Figs. 1 and 2.

1. The X^2A'' state

The potential energy surface along the ClO bond stretching coordinate (Fig. 1) is broad and shallow as would be expected for a weak bond. The surface exhibits a weak double minimum character but this is probably due to CSF selection noise (*vide supra*).

The electronic binding energy relative to that of Cl + O₂ products is calculated to be approximately 0.01 hartree (6 kcal/mol) in agreement with the experimental value of 7.6 kcal/mol. However, the present treatment is focused on providing a description of several excited states and this results in a rather large uncertainty ($\pm 100\%$) in the computed D_e . The natural orbital CI, which should be somewhat more accurate, gave similar results (Table II). We, therefore, estimate that $D_e = 7.5 \pm 4$ kcal/mol.

The shape of the potential along the O-O stretching coordinate (Fig. 2) appears much more conventional and the curvature near the bottom of the well agrees with Arkell and Schwager's experimental force constant for the O-O stretch. The calculations indicate that ground state is bound by 3.46

TABLE II. CI energies of the X^2A'' state using approximate natural orbitals.^a

R (ClO)	R (OO)	< ClOO	E
3.1	2.48	113.6	-609.2673
3.3	2.48	113.6	-609.2796
3.45	2.48	113.6	-609.2841
3.6	2.48	113.6	-609.2867
3.75	2.48	113.6	-609.2874
3.9	2.48	113.6	-609.2844
4.1	2.48	113.6	-609.2860
4.3	2.48	113.6	-609.2848
4.5	2.48	113.6	-609.2829
5.0	2.48	113.6	-609.2783
7.0	2.48	113.6	-609.2742
25.0	2.40	180.	-609.2774
3.60	2.20	113.6	-609.2681
3.60	2.48	113.6	-609.2867
3.60	2.60	113.6	-609.2745
3.75	2.20	105.	-609.2755
3.75	2.48	105.	-609.2847
3.75	2.60	105.	-609.2785
3.75	2.36	113.6	-609.2887
3.75	2.48	122.	-609.2892
3.60	2.60	105.	-609.2831

^a Bond lengths in bohr, angles in degrees, and energies in hartrees.

eV relative to dissociation to ClO and O. This value should be reduced by ~ 0.8 eV to account for relaxation of the ClO bond length at dissociation.¹⁵ The resulting value, when compared to the difference between the dissociation energies of ClO and O₂ gives ~ 7 kcal/mol for the binding energy of ClO relative to ClO + O₂ in (fortuitously) good agreement with the value obtained by direct calculation. The ground state dipole moment is relatively small (~ 0.1 a.u.) in the equilibrium region (Table III). At shorter bond lengths the charge transfer and resulting dipole moment increases.

2. The ${}^2A''$ excited states

The most important feature of the three ${}^2A''$ excited states treated is that they are strongly repulsive with respect to dissociation into Cl and O₂ fragments (Fig. 1). All three of the ${}^2A''$ excited states lie in a narrow band in the equilibrium region. The vertical excitation energies are calculated to fall in the range 2.0 to 3.8 eV with an uncertainty of ~ 0.3 eV. The first excited state dissociates to the ground state asymptote, (2P) Cl + (${}^3\Sigma_g^-$) O₂, while the second and third excited states apparently yield (${}^1\Delta_g$) O₂.

The behavior of the ${}^2A''$ states as a function of the O-O bond length is shown in Fig. 2 for fixed values of R (ClO) and \angle ClOO. A barrier to dissociation of the ${}^2A''$ state to ClO + O is predicted to occur at $\sim R$ (OO) = 3.5 bohr. If the R (Cl-O) bond length is relaxed at R (O-O) = 3.5, the barrier is predicted to be 0.7 eV. In addition, if the ClO potential energy of Arnold, Whiting, and Langhoff¹⁵ is used to estimate the energy lowering which would be obtained by relaxing the ClO bond length at infinite R (O-O), the ${}^2A''$ state is found to be slightly metastable. Due to the uncertainties in the present energies, this prediction is not definitive. The second and third excited ${}^2A''$ states also exhibit a potential well with respect to R (O-O) in the equilibrium region.

The third excited ${}^2A''$ state has a maximum at $\sim R$ (O-O) = 3.1 bohr which, on the basis of the transition moment to the ground state (*vide infra*), is apparently due to an avoided crossing with a higher state. An avoided crossing occurs between the $3^2A''$ and $2^2A''$ states near R (O-

TABLE III. Dipole moment of the X^2A'' state.^a

R (ClO)	R (OO)	ClOO	M, MSCSF	M, CI
3.75	2.48	95	0.045	0.124
3.75	2.48	105	0.046	0.111
3.75	2.48	113.6	0.051	0.105
3.75	2.48	122	0.056	0.110
3.6	2.0	113.6	0.358	0.579
3.6	2.2	113.6	0.071	0.279
3.6	2.48	113.6	0.091	0.027
3.6	2.6	113.6	0.120	0.060
3.6	2.8	113.6	0.145	0.147
3.6	3.1	113.6		0.227
3.6	3.5	113.6	0.151	0.197
3.3	2.48	113.6	0.202	0.327
3.45	2.48	113.6	0.145	0.109
3.9	2.48	113.6	0.037	0.147
5.0 ^b	2.48	113.6	0.041	0.107

^a Dipole moment in atomic units, bond lengths, in bohr, and angles in degrees.

^b Single excitations which were rejected during configuration selection were not retained in this calculation.

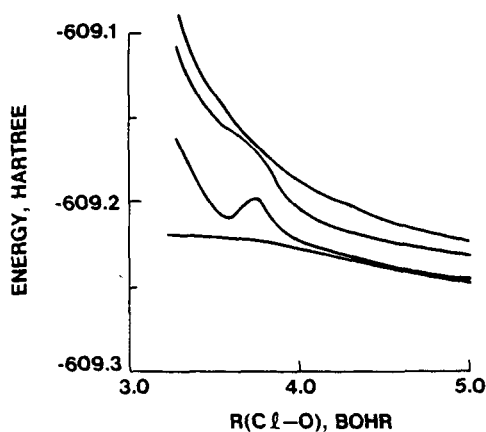


FIG. 3. CI energies of the ${}^2A'$ states as a function of $R(\text{ClO})$. The ClOO angle and $R(\text{OO})$ bond length are the same as those given in Fig. 2.

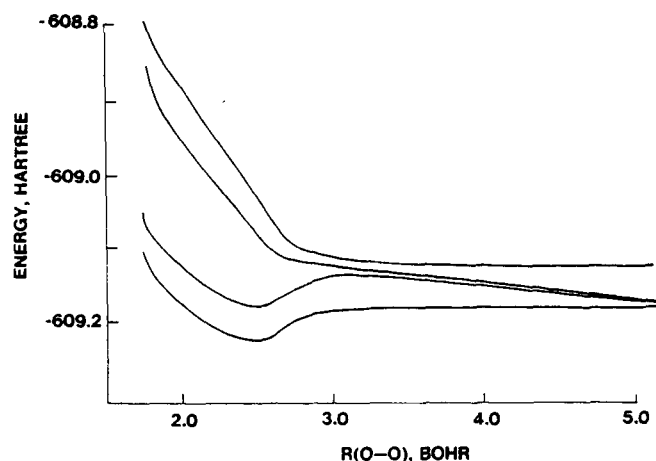


FIG. 5. CI energies of ${}^4A''$ states as a function of $R(\text{OO})$. The ClOO angle and ClO bond lengths are the same as those given in Fig. 3.

$\text{O}) = 3.5$ bohr. The character of the ${}^2A''$ excited states changes drastically for $R(\text{O-O}) \geq 3.5$ bohr. At $R(\text{O-O}) = 5$ bohr the first three ${}^2A''$ states are converging to ground state products while the energy of the ${}^4A''$ state indicates that it dissociates to yield $\text{O}({}^1D)$.

The bending potentials for the ${}^2A''$ excited states (Table I) exhibit an orbital basis artifact for the excited states. However, aside from this artifact, the two lowest ${}^2A''$ excited state bending potentials are relatively flat. Several calculations (Table I) were carried out to explore the possibility of a low energy channel for dissociation to $\text{ClO} + \text{O}$. No lower energy channel for dissociation of the excited states to these products was revealed by these calculations.

B. ${}^2A'$ states

Slices through the ${}^2A'$ potential surfaces along the $R(\text{ClO})$ and $R(\text{OO})$ coordinates are shown in Figs. 3 and 4. As with the ${}^2A''$ excited states, all four of the ${}^2A'$ states were repulsive with respect to dissociation into Cl and O_2 , had bound regions with respect to dissociation into $\text{ClO} + \text{O}$,

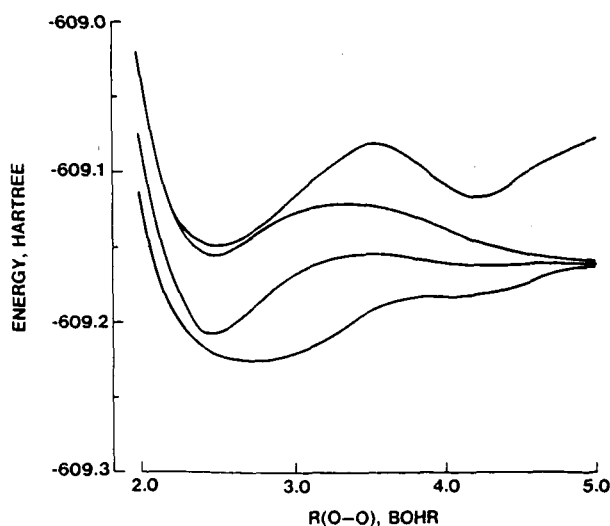


FIG. 4. CI energies of the ${}^2A'$ states as a function of $R(\text{OO})$. The ClOO angle and ClO bond length are the same as those given in Fig. 3.

and exhibited an artifact "bump" in the bending potentials due to the orbital bias. This bump is evident in the ClO stretch potential for the ${}^2A'$ state (Fig. 3) at $R(\text{ClO}) = 3.75$ bohr. Neglecting the artifact, the bending potentials (Table I) of the ${}^2A'$ states appear relatively flat. The behavior of the potentials at small angles may be indicative of a low energy path between the excited states of ClOO and OClO. The first two ${}^2A'$ states lie below the ${}^2A''$ state. The existence of one low lying ${}^2A'$ state is expected on the basis of the near infrared spectra of HO_2 and other peroxy compounds. The first three ${}^2A'$ states dissociate to ground state products on the $R(\text{ClO})$ coordinate and the 4th ${}^2A'$ state produces $({}^1\Delta_g)\text{O}_2$. On the $R(\text{OO})$ coordinate the first three states yield ground state products while the fourth dissociates to ground state ClO and $({}^1D)\text{O}$. However, the third and fourth states are predicted to have intersections on both the inner and outer limbs so the fourth state may be effectively predissociated to ground state products.

In summary, the ${}^2A'$ states investigated are expected to lead to absorption in the 1.5 to 5 eV region. The quantum yield should be unity for the entire spectral range. The pho-

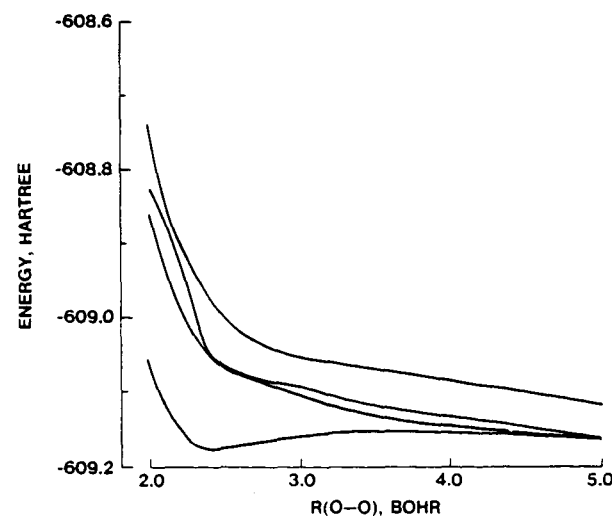


FIG. 6. CI energies of the ${}^4A'$ states as a function of $R(\text{OO})$. The ClOO angle and the ClO bond length are the same as those given in Fig. 3.

TABLE IV. Transition moments between X^2A'' and the doublet excited states,^a

R (ClO)	Geometry		Upper state							
	R (OO)	ClOO	$2^2A''$	$3^2A''$	$4^2A''$	$1^2A''$	$2^2A'$	$3^2A'$	$4^2A'$	
3.1	2.48	113.6	0.433	0.116	1.035					
3.3	2.48	113.6	0.208	0.112	0.066	0.090	0.148	0.030	0.308	
3.6	2.48	113.6	0.063	0.081	0.035	0.014	0.002	0.007	0.069	
3.75	2.48	113.6	0.062	0.053	0.025	0.012	0.010	0.046	0.030	
3.90	2.48	113.6	0.042	0.032	0.023	0.005	0.003	0.040	0.002	
5.0	2.48	113.6	0.032	0.032	0.010	0.044	0.019	0.007		
3.6	2.0	113.6	0.045	0.050	0.058	0.005	0.005	0.074	0.005	
3.6	2.7	113.6	0.037	0.037	0.043					
3.6	2.8	113.6	0.080	0.078	0.008	0.006	0.011	0.047	0.036	
3.6	3.1	113.6	0.073	0.050	0.276	0.005	0.013	0.030	0.021	
3.6	3.5	113.6	0.010	0.038	0.041	0.003	0.008	0.001	0.025	
3.75	2.48	95	0.022	0.255	0.139	0.014	0.003	0.043	0.019	
3.75	2.48	105	0.042	0.123	0.063	0.011	0.003	0.050	0.017	
3.75	2.48	122	0.060	0.036	0.021	0.007	0.001	0.024	0.002	

^a Transition moments in atomic units.

tolysis products are predicted to be entirely Cl + O₂ in the visible and near UV region and predominately these products in the higher energy region (> 3.5 eV) where the channel for ClO + O production is open.

C. Quartet states

The behavior of the four lowest A'' and A' quartet states were investigated along the R (OO) coordinate. The results, which are given in Figs. 5 and 6, show the first two $4A''$ states and the lowest energy $4A'$ state to be bound with respect to dissociation into ClO + O. The remaining five quartet states are repulsive with respect to dissociation into ClO + O. The three lowest states of each symmetry dissociate to ground state products while the fourth state in each symmetry apparently dissociates to higher states of the products. The repulsive quartet states predissociate the fourth $2A''$ and $2A'$ states. Since the latter states are repulsive with respect to dissociation to Cl + O₂, the quartet states are not expected to be important to the photodissociation of any of the states investigated here, but many may be significant for O + ClO collisions. In particular, reactive scattering on the $1^4A''$ surface may be responsible, in part, for the difference between the theoretical⁷ and experimental⁸ results for the rate of the reaction (*vide infra*).

D. Transition moments

The transition moments for the $2A''$ and $2A'$ excited states are given in Table IV for several geometries. The transition moments are quite small near the ground state equilibrium geometry and become even smaller at larger values of R (ClO) as would be expected for excited states arising from the ground state of Cl and the ground and 1^4A_g states of O₂. The calculated values of R (ClO) = 5.0 bohr are a little larger than they should be because forced retention of single excitation was not used at that geometry.

The transition moments become somewhat larger for ClO bond lengths and bond angles smaller than the values for the ground state equilibrium. The larger value obtained for the transition moment to the $4^2A''$ state of R (O-O) = 3.1

bohr is indicative of mixing between the state and a higher state of the same symmetry and may explain the behavior of the $4^2A''$ energy in that region.

These results indicate that the absorption of ClOO will be quite weak in the visible region. The intensity of the solar spectrum in the visible region will substantially enhance the importance of this weak absorption with regard to atmospheric processes. However, since the products of photodissociation at longer wavelengths are Cl and O₂, the net effect of photodissociation will be to slightly enhance the total rate of dissociation to these products; a process which is dominated by the high rate of thermal dissociation.

IV. DISCUSSION

A. Photochemistry of ClOO

The repulsive nature of the lower doublet states of ClOO on the ClO coordinate should dominate the photochemistry for wavelengths in the visible and near UV. The absorption strength at shorter wavelengths will involve states that were not included in the present investigation. The calculated vertical excitation energies for the states included in the present treatment range from approximately 1.8 to 3.2 eV. The extent of the energy range of the absorption system due to these states will depend on the spatial extent of the nonzero amplitude of the lower vibrational levels of the ground state. Although the present ground state results are not sufficiently accurate to establish the latter, the system probably extends from between 4 and 5 eV down to about 1.5 eV. Although it is possible to estimate the spectrum on the basis of harmonic oscillator vibrational functions chosen to reproduce the experimental ClO stretching frequency, such an estimate could err significantly near the absorption edges, particularly if the actual potential is quite anharmonic. Since the products of photolysis are the same as those of the rapid thermal dissociation, photolysis of ClOO should not have a significant effect in atmospheric chemistry.

Arkell and Schwager^{11a} observed photo-isomerization of OClO to ClOO. The absence of significant repulsion in the small angle portion of the potential energy surfaces of several excited states appears to provide a mechanism for the photo-isomerization. The repulsive nature of the ClOO excited

states explains these authors failure to observe the reverse process. Arkell and Schwager suggested that the loss of ClOO observed at temperatures (above 20 K) high enough for the Cl atoms to be mobile might have been due to photolysis (to Cl + O₂) by the infrared source in their spectrophotometer. At lower temperatures the lattice cage effects would lead to immediate recombination of the photolysis products.

The remaining observation by Arkell and Schwager which is of interest here is their assignment of infrared lines at 435 and 1414 cm⁻¹ to a third isomer of ClO₂. Their results indicated that this species was produced by the photolysis of OCIO and converted to ClOO upon warming above 4 K. They assigned this species as a geometrical isomer of ClOO because the isotopic splittings indicated that it was unsymmetrical and its lifetime at 20 K was too long to support its assignment to a metastable electronic state. The present results suggest two possibilities for this species: (1) that the double minimum nature calculated for the ground state is real and that the metastable isomer corresponds to the higher energy of the two minima; and (2) that there exists a metastable region in the small ClOO angle portion of the 1²A' surface. As noted earlier, the shallow double minimum in the ground state is probably an artifact of the computational techniques. In order for the latter possibility to satisfy all of the experimental constraints, the metastable 1²A' state geometry would have to correspond to a distorted ring state and would have to lie below the 1²A'' state in that conformation. Although the present calculations did not provide definitive evidence that the latter possibility is fulfilled, the shapes of the computed surfaces indicate that it might exist.

We conclude this section by again pointing out that although the photochemistry of ClOO involves a large number of relatively low lying states, the repulsive nature common to the lowest doublet excited states is expected to be the dominant factor.

B. Comparison of the states of ClOO and HOO

It is useful to compare the results for ClOO, about which little was previously known, to those of HO₂. HO₂ is the simplest peroxy compound and has been the subject of several experimental¹⁶ and theoretical¹⁷ investigations. The similarities in the gross electronic structure of the O₂ fragment and in the observed¹⁸ low energy $X^2A'' \leftarrow 1^2A'$ transition of several peroxy compounds has led to the states of HO₂ being used as a model for understanding the electronic spectra of other peroxy compounds. Some similarities also exist between the observed UV spectra of HO₂ and ClOO.³

Although the transition moments are larger at the conformations which would lead to absorption in the quartz UV region investigated by Johnston *et al.*,³ the Franck-Condon factors for these are small. Poorly converged results for higher states (above the 4²A'' and 4²A' states) indicate that these higher states of ClOO are probably primarily responsible for the absorption observed at ~2500 Å. The transition moment obtained for the transition to the 4²A'' state at the avoided crossing with the 5²A'' at $R(\text{OO}) = 3.1$ bohr indicates that transitions to these higher states carry a larger intensity.

The ClOO molecule also has a relatively low lying 1²A' state, but the present results indicate that it is repulsive with respect to dissociation into Cl + O₂ and it has not been observed experimentally. Also, the gross similarity of the UV spectra of ClOO and HOO is fortuitous. The UV absorption in HOO is due to transitions to the 2²A'' and 2²A' states which are metastable with respect to breaking the X-O bond and repulsive with respect to the O-O bond coordinate. These states lie at lower energies in ClOO and exhibit the opposite behavior with respect to the shape of the surfaces. The $X^2A'' \rightarrow 2^2A''$ transition carries considerable intensity in HOO, but is quite weak in ClOO. The differences between the electronic states of these structurally similar molecules arise from several factors, but the major factor is the weakness of the ClO bond. This leads to a small splitting between the bonding and antibonding orbitals for this bond, lowering the energy of $\sigma(\text{ClO}) \rightarrow \sigma^*(\text{ClO})$ excitation and the excitations from the lone pair orbital on the terminal oxygen to the ClO antibonding orbital. The low energy of the latter results in this transition being effective in back donating electron density in the σ space to compensate for charge transfer in the pi orbital space. It is the latter which is responsible for the ionicity^{17(c),17(d)} of the 2²A'' state of HO₂. The magnitude of the transition moment between the lower 2²A'' states in HOO is due to this ionicity,^{17(d)} which is largely absent in ClOO. The dipole moment of the 2²A'' state of ClOO at the ground state equilibrium geometry is only 0.98 D, whereas the dipole moment of the 2²A'' state of HOO is 4 D.^{17(d)} The transitions from the lone pair electrons on Cl also contribute to the dense spectrum of states in the visible through quartz UV regions, compared to that of HOO.

C. Other peroxy molecules

The infrared spectrum¹⁹ of FOO indicates that the FO bond is weak. Since it has the same number of valence electrons as ClOO and is structurally similar, its spectrum and photolysis products would be expected to be similar to those predicted here for ClOO. A long wavelength band ($300 < \lambda < 600$ nm with $\lambda_{\text{max}} \sim 420$ nm) has been observed²⁰⁻²² for FOO and the photolysis products (above ~490 nm in argon matrix) are reported²² to be F + O₂. A shorter wavelength band $\lambda_{\text{max}} \sim 205$ nm has also been observed, but the photolysis products are now known. The theoretical results obtained here for the lower energy transitions in ClOO provide support for the experimental assignments of the observed long wavelength band to FOO and for assignment of the products in that band to F + O₂.

The CO bond strength in CH₃O₂ is apparently subject to a large uncertainty. If the 3s electrons of the Cl atom are included in the valence shell, CH₃O₂ is formally iso-valence-electronic to ClOO, but there are significant differences between the lone pairs of Cl and the bonding orbitals of CH₃. Experimental evidence¹⁸ indicates that the low lying 1²A' state (assuming C_s symmetry) is bound in CH₃O₂ and a short wavelength band has been observed. The former suggests that at least two states of CH₃O₂ are similar to those of HO₂, but the question regarding the photolysis products and of the existence of longer wavelength absorption are not resolved experimentally. These questions are significant for the atmo-

spheric chemistry of CH_3O_2 in the relatively clean troposphere. Photolysis may compete with reactions of CH_3O_2 with other trace species if it possesses absorption beyond 300 nm and would be important if it results in products other than $\text{CH}_3 + \text{O}_2$.

D. The $\text{ClO} + \text{O} \rightarrow \text{Cl} + \text{O}_2$ reaction

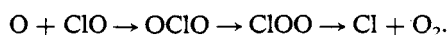
This reaction, which closes the loop in the catalytic destruction of ozone by Cl, was the subject of several experimental investigations⁸ and a theoretical investigation by Jaffe.⁷ The experimental investigations^{8(a),8(b)} gave opposite temperature effects and the theoretical rate was lower than the experimental values.

Jaffe's trajectory calculations on the $\text{ClO} + \text{O} \rightarrow \text{Cl} + \text{O}_2$ reaction utilized several assumptions regarding the states of the ClOO intermediate. These included assuming that; (a) the topography of the ground state and the $1^2A'$ state are similar so that the ground state potential could be used for both states; (b) the lowest quartet states are unreactive; and (c) that the shape of the surfaces are such that the OCIO region is not accessible at low temperature. The present results indicate that the bending potential for the $1^2A'$ is quite flat so that assumption (a) would result in some underprediction of the reaction rate. However, Jaffe discounted (a) somewhat by using effective bending force constants of 1/2 and 1/4 the experimental $^2A'$ value for some of his calculations. The flat bending potential for the $1^2A'$ state also suggests that assumption (c) may be inappropriate.

The present results are not sufficiently complete to enable more than speculation on the latter point. The observations⁴ of thermal isomerization and photoisomerization in certain matrices are also suggestive, but not definitive in this regard. The net effect of introducing a low energy channel to the OCIO surface is not clear since it would result in processes which would reduce the calculated rate (especially at high temperatures)



as well as those which would increase the calculated rate



The present calculations indicate that the $1^4A''$ state does not have a large barrier in the entrance channel so that assumption (b) should contribute to an underprediction of the rate by the trajectory calculations. Neither the exit channel nor the bending portions of the surface were investigated here, but it is relatively safe to assume that the exit channel has the same repulsive character as the doublet excited states.

The present results appear to qualitatively explain the underprediction of the low temperature rate by Jaffe's trajectory calculations. Because of the three surfaces contributing to the low temperature rate, the additional surfaces which would become important at high temperatures, and the possibility that both OCIO and ClOO intermediates may be involved; the mechanism cannot be regarded as being simple. Some additional calculations on the potential energy surfaces and more elaborate trajectory calculations would be required to resolve the uncertainties²² regarding this reaction.

E. Other reactions

Although reactions between ClOO and other species were not investigated directly in the present work, the information on the bonding and electronic properties does facilitate speculation on ClOO reactions.

The weak ClO bond and near normal O_2 bond would suggest that reactions like



should be significantly slower than similar reactions involving HO_2 . On the other hand, the weakness of the ClO bond in ClOO should facilitate the extraction of the Cl atom in reactions like



The ratio of the rates of reactions (6) and (7) when $\text{X} = \text{Cl}$ as well as the comparison of the rates of the $\text{Cl} + \text{HOO}$ and $\text{Cl} + \text{ClOO}$ reactions seem to support this rational. Indeed, the present results suggest that ClOO might be best viewed as a Cl atom "chaperoned" by an O_2 molecule. From this point of view reaction (7) would be a chaperoned Cl addition rather than an abstraction reaction. Since the equilibrium between $\text{Cl} + \text{O}_2$ and ClOO favors the free Cl atom under atmospheric conditions, and since ClOO is expected to react like a (chaperoned) Cl atom, the ClOO reaction rates would have to be at least two orders of magnitude faster than equivalent Cl atom reactions in order to compete with the latter. This might occur in cases where the chaperone caused a chlorine addition to be biomolecular rather than termolecular.

Although there are a number of possible reactions of this type involving OH, HO_2 , NO, NO_2 , and NO_3 which might have some significance under the conditions of laboratory investigations, none of them would seem to be important under average daylight atmospheric conditions. For example, the reaction between ClOO and OH yielding $\text{HOCl} + \text{O}_2$ would be expected to have a rate similar to that for the $\text{Cl} + \text{ClOO} \rightarrow \text{Cl}_2 + \text{O}_2$ reaction ($k \sim 1 \times 10^{-10} \text{ cm}^3 \text{ molecule}^{-1} \text{ s}^{-1}$), but the formation of HOCl by this mechanism would be orders of magnitude lower than by the $\text{ClO} + \text{HO}_2$ reaction and the rate of removal of free Cl would be insignificant. The ClOO reactions with NO and NO_2 may compete with the third order Cl atom addition reactions, but in this case the products are photolyzed rapidly and are not thought to be important in the atmosphere.

¹[a] R. G. W. Norrish and G. H. J. Neville, *J. Chem. Soc.* **1934**, 1864; (b) M. A. A. Clyne and J. A. Coxon, *Proc. R. Soc. London Ser. A* **303**, 207 (1968); (c) J. E. Nicholas and R. G. W. Norrish, *ibid.* **A 307**, 391 (1968).

²R. G. Prinn, *J. Atmos. Sci.* **28**, 1058 (1971).

³H. S. Johnston, E. D. Morris, Jr., and J. Van den Bogaerde, *J. Am. Chem. Soc.* **91**, 7712 (1969).

⁴[a] R. S. Eachus, P. R. Edwards, S. Subramanian, and M. C. R. Symons, *J. Chem. Soc. A* **1968**, 1704; (b) A. Arkell and I. Schwager, *J. Am. Chem. Soc.* **89**, 599 (1967).

⁵R. F. Hampson, U. S. Dept. Trans. Report No. FAA-EE-80-17 (1980).

⁶J. L. Gole and E. F. Hayes, *Int. J. Quantum Chem* **III**, 519 (1970).

⁷R. L. Jaffe, *Chem. Phys.* **40**, 185 (1979).

⁸[a] M. S. Zahnisen and F. Kaufman, *J. Chem. Phys.* **66**, 3673 (1977); (b) M. A. A. Clyne and W. S. Nip, *J. Chem. Soc. Faraday Trans. 1* **72**, 2211

- (1976); (c) P. P. Bernard, M. A. A. Clyne, and R. T. Watson, *ibid.* **69**, 1356 (1973).
- ⁹Van Duijneveldt, IBM Res. Rep. RJ945, 1971.
- ¹⁰S. Huzinaga, D. McWilliams, and D. Domsy, *J. Chem. Phys.* **54**, 2283 (1971).
- ¹¹R. C. Raffanetti, *J. Chem. Phys.* **58**, 4452 (1973).
- ¹²G. Hirsch, P. J. Bruna, S. T. Peyerimhoff, and R. J. Beunker, *Chem. Phys. Lett.* **52**, 442 (1977).
- ¹³(a) J. S. Wright and R. J. Williams, *Theor. Chem. Acta. (Berlin)* **65**, 59 (1984); (b) R. C. Raffanetti, K. Hsu, and I. Shavitt, *Theor. Chem. Acta.* **45**, 33 (1977).
- ¹⁴R. C. Raffanetti and D. H. Phillips (unpublished results on H₂O and H₂O⁺).
- ¹⁵J. O. Arnold, E. E. Whiting, and S. R. Langhoff, *J. Chem. Phys.* **66**, 4459 (1977).
- ¹⁶(a) H. E. Hunziker and H. R. Wendt, *J. Chem. Phys.* **60**, 4622 (1974); (b) T. T. Paukert and H. S. Johnston, *ibid.* **56**, 2825 (1972).
- ¹⁷(a) J. G. Gole and E. F. Hayes, *J. Chem. Phys.* **57**, 360 (1972); (b) R. J. Buenker and S. D. Peyerimhoff, *Chem. Phys. Lett.* **37**, 208 (1976); (c) W. A. Goddard III, *Lecture Notes, School on the Fundamental Chemical Basis of Reactions in the Polluted Atmosphere*, edited by C. W. Kern (Battelle Research Center, Seattle, Washington, 1973); (d) S. R. Langhoff and R. L. Jaffe, *J. Chem. Phys.* **71**, 1475 (1979).
- ¹⁸H. E. Hunziker and H. R. Wendt, *J. Chem. Phys.* **64**, 3488 (1976).
- ¹⁹(a) R. D. Sprately, J. J. Turner, and G. C. Pimentel, *J. Chem. Phys.* **44**, 2063 (1966); (b) A. Arkel, *J. Am. Chem. Soc.* **87**, 4057 (1965).
- ²⁰R. W. Fessenden and R. H. Schuler, *J. Chem. Phys.* **44**, 434 (1966).
- ²¹N. M. Matchuk, V. I. Tupikov, A. I. Malkova, and S. Ya. Pshezhetskii, *Opt. Spectrosc.* **40**, 7 (1976).
- ²²M. E. Jacox, *J. Mol. Spectrosc.* **84**, 74 (1980).

ON THE USE OF CORRESPONDING ORBITALS IN THE CALCULATION
OF NONORTHOGONAL TRANSITION MOMENTS

LENGSFIELD, JAFRI, PHILLIPS & BAUSCHLICHER

Reprinted from JOURNAL OF CHEMICAL PHYSICS
Vol. 74, No. 12, pp. 6849-6856 June 15, 1981
Published by THE AMERICAN INSTITUTE OF PHYSICS
For the Journal of Chemical Physics.

On the use of corresponding orbitals in the calculation of nonorthogonal transition moments

Byron H. Lengsfeld, III,^{a)} Jawed A. Jafri, and Donald H. Phillips

NASA Langley Research Center, Hampton, Virginia 23665

Charles W. Bauschlicher, Jr.^{b)}

Institute for Computer Applications in Science and Engineering, NASA Langley Research Center, Hampton, Virginia 23665

(Received 23 July 1980; accepted 13 February 1981)

Full valence and first-order CI wave functions are invariant with respect to unitary transformations among the valence orbitals. We exploit this degree of freedom and show that by transforming the valence orbitals into a corresponding orbital basis, nonorthogonal transition moment calculations become an easily managed task. Sample full valence calculations on several states of O_2^+ and OF are also presented.

INTRODUCTION

The computational difficulties involved in calculating the transition moments between CI wave functions which are composed of nonorthogonal orbitals are well known.^{1,2} These difficulties arise from the need to compute the cofactors of the overlap matrices associated with most pairs of determinants comprising the two CI wave functions. This problem vanishes if the same molecular orbitals can be employed in both CI wave functions. Unfortunately, the low-lying states of a large number of molecules are not well described by the same orbital basis, e. g., BeO and MgO.³ In the case of a limited CI expansion the nonorthogonal transition moments can be obtained without excessive computational effort.^{4,5} For larger systems, the bounds on a transition moment can be estimated by performing orthogonal calculations with both sets of orbitals. More rigorous bounds to the transition moment can be obtained from techniques developed by Weinhold⁶ and extended by Langhoff and Chong.⁷

In this paper, we show that the computational difficulties encountered in nonorthogonal transition moment calculations involving full valence, first-order and to a lesser degree second-order CI wave functions can be greatly reduced by exploiting the invariance of the CI wave functions with respect to unitary transformations among the valence orbitals. In this algorithm the same core orbitals are employed in both states and the valence orbitals of the two states under investigation are transformed to a corresponding orbital basis.⁸ As a result of the simple nature of the overlap matrix, the calculation of a nonorthogonal transition moment becomes an easily managed task.

The ability to compute nonorthogonal transition mo-

ments for a complete active space (CAS) wave function with little work in excess of that needed to obtain the orthogonal transition moment is especially useful in light of the recent advances by Roos⁹ and Siegbahn¹⁰ on efficient methods to perform large CAS MCSCF's. Moreover, recent studies of the alkaline earth oxides have indicated that the orbitals needed to compactly describe the ground state and the low-lying excited states are significantly different.^{2,3} Clearly, any method which can be efficiently employed to obtain the nonorthogonal transition moments for such systems are very useful indeed.

Corresponding orbitals have been employed extensively in connection with projected-unrestricted-Hartree-Fock calculations,¹¹ but they have rarely been employed in connection with CI calculations. The notable exceptions are the work of Davidson and Martin¹² in which corresponding orbitals were exploited for interpretative purposes and the work of Bagus¹³ where corresponding orbitals were used in the study of localized solutions in core ionized systems.

King¹⁴ has used corresponding orbitals as an alternative to the method of Prosser and Hagstrom¹⁵ for computing the matrix elements in nonorthogonal CI and transition moment calculations. In King's method a different set of corresponding orbitals are determined for most determinant-determinant interactions.

CALCULATION OF TRANSITION MOMENTS

Our goal is to compute the transition moment (TM) between two states ψ_1 and ψ_2 :

$$TM = \langle \psi_1 | x, y, \text{ or } z | \psi_2 \rangle .$$

The most direct way to proceed is to compute the transition density matrix¹⁶ (TDM), and then take the trace of the dipole integrals and the TDM to obtain the TM. In practice, ψ is a linear combination of CSF's

$$\psi_I = \sum_j CI_j^I * CSF_j^I ,$$

and each CSF is a linear combination of determinants

$$CSF_j^I = \sum_k C_j^I(k) * DET^I(k) .$$

^{a)}NASA-NRC Postdoctoral Fellow 1978-1980. Present address: IBM Research Laboratory, 5600 Cottle Road, San Jose, Calif. 95193.

^{b)}This report was prepared as a result of work performed by this author under NASA Contract No. NAS1-14472 and NAS1-15810 while in residence at ICASE, NASA Langley Research Center, Hampton, Va. 23665. Present address: Polyatomic Research Inc. 1101 San Antonio Road, Mt. View, Calif. 94043.

For wave functions of this type, the contribution of each determinant-determinant interaction [weighted by the appropriate CI_i 's and $C_j(k)$'s] is determined and added to the TDM. If we let m denote an occupied orbital in the one determinant and n denote an occupied orbital in the other, then each contribution to the TDM can be expressed as follows:

$$\text{TDM}(m, n) = \sum_{i,j} CI_i^m CI_j^n \sum_{o,p} C_i^m(o) C_j^n(p) \Delta_{mn}^{op},$$

where Δ_{mn}^{op} is the cofactor of the o, p determinant-determinant overlap matrix.

In the most general case of nonorthogonal orbitals, Δ_{mn} is nonzero and the contributions from each pair of determinants must be evaluated. The inclusion of symmetry gives rise to some savings, but the amount of work is still very large.

The use of orthogonal orbitals represents a large reduction in work, since Δ_{mn} is either zero, one, or minus one, and most of the zero detection can be accomplished at the occupation level. Only identical occupations or occupations which differ by one orbital need be processed. Because a cofactor need not be evaluated for every determinant-determinant interaction, an algorithm can be designed to evaluate orthogonal transition moments in which very little work is performed at the determinantal level.

A third possibility is to employ corresponding orbitals as the one-particle basis in the CI calculations. Corresponding orbitals are defined by the following overlap properties^{8,14}:

$$\langle a_i | a_j \rangle = \langle b_i | b_j \rangle = \delta_{ij} \quad (1a)$$

and

$$\langle a_i | b_j \rangle = d_i \delta_{ij} \quad (1b)$$

Given two sets of orbitals (X_i) and (Y_i) the corresponding orbitals $\{a_i\}$ associated with (X_i) are obtained by diagonalizing:

$$\bar{G} = \bar{S}^{xy} (\bar{S}^{xy})^* \quad (2)$$

where $S_{ij}^{xy} = \langle X_i | Y_j \rangle$ and i, j are valence (active) orbitals. The corresponding orbitals $\{b_i\}$ associated with (Y_i) can be obtained by diagonalizing: $\bar{S}^{yx} (\bar{S}^{yx})^t$. However, this procedure can fail to yield a diagonal overlap matrix if degenerated eigenvalues are present. This problem can be solved by diagonalizing \bar{G} to obtain one set of corresponding orbitals and then obtain the second set by means of a projection operator¹⁷:

$$\bar{P}^y | a_i \rangle = \sum_j | Y_j \rangle \langle Y_j | a_i \rangle \quad (3a)$$

$$= \sum_j | b_j \rangle \langle b_j | a_i \rangle = d_i | b_i \rangle \quad (3b)$$

The diagonal overlap matrix associated with the corresponding orbital basis can be used to detect zero contributions to the TDM at the occupation level and also at the determinantal level. Moreover, the simple structure of the overlap matrix greatly reduces the computational effort required to evaluate the cofactors. Thus, in the CI studies where corresponding orbitals can be

employed, it is possible to perform a nonorthogonal TM calculation with only slightly more work than the effort required to obtain the comparable orthogonal TM.

We should note that if one is interested in calculating the TM between several states, the corresponding orbitals between each pair of states must be determined and the CI calculations repeated in this basis. However, we find with our CI that the time to evaluate the wave functions is usually less than the time to compute the nonorthogonal TDM.

FULL VALENCE CI

In a full valence CI calculation, the energy is invariant to unitary transformation among the valence orbitals. One is then free to choose the orbital basis which reduces the computational effort needed to obtain the transition moment. This task can be accomplished very easily if the overlap matrix between the occupied orbitals of the two states is diagonal. The orbitals which satisfy this overlap criteria are simply the corresponding orbitals. Because of the diagonal nature of the overlap matrix, two occupations which differ by two or more orbitals do not contribute to the TDM and are not processed. In fact, these calculations are performed in the same manner as an orthogonal transition moment computation, the only difference being that one multiplies each contribution of the TDM which would arise in an orthogonal calculation by a cofactor of the overlap matrix. These cofactors are particularly simple to obtain, as every nonzero cofactor is of the form

$$\text{CF}(i) = \frac{1}{d_i} \left\{ \prod_j d_j \right\} \quad (4a)$$

$$= \prod_{k \neq i} d_k \quad (4b)$$

where the product extends over all of the spin orbitals in one of the interacting occupations. It is convenient to precompute the terms in brackets in Eq. (4a) for every occupation appearing in one of the CI wave functions. If one of the d_i 's appearing in Eq. (4a) is zero, then one precomputes the product defined by Eq. (4b). A key is also constructed to indicate which orbital possesses a zero overlap, as only this orbital is involved in the nonzero contributions to the TDM. If two or more of the d_i 's are zero, then this occupation cannot contribute to the TDM.

Thus, in the full valence case the nonorthogonal TM is evaluated in virtually the same time as the orthogonal TM. This is very useful for CAS MCSCF wave functions.

FIRST-ORDER CI

Corresponding orbitals may also be utilized to great advantage in the calculation of transition moments involving first-order CI (FOCI)¹⁸ wave functions. The formulas for the cofactors which occur in a FOCI calculation are naturally more complicated than those encountered in a full valence calculation. However, these formulas represent a significant reduction of work when

$$\begin{array}{c}
 b'_1 \\
 b'_2 \\
 w'_1 \\
 b''_1 \\
 b''_2 \\
 b''_3
 \end{array}
 \left(
 \begin{array}{cccc|cc}
 a'_1 & a'_2 & a'_3 & v'_1 & a''_1 & a''_2 \\
 d'_1 & 0 & 0 & c'_1 & 0 & 0 \\
 0 & d'_2 & 0 & c'_2 & 0 & 0 \\
 e'_1 & e'_2 & e'_u & f & 0 & 0 \\
 \hline
 0 & 0 & 0 & 0 & d''_1 & 0 \\
 0 & 0 & 0 & 0 & 0 & d''_2 \\
 0 & 0 & 0 & 0 & 0 & 0
 \end{array}
 \right)
 = S \quad .$$

\uparrow
 a_u

-ZO

Once again, the nonzero cofactors of the overlap matrix arise from the exclusion of row 6 and one of the first four columns. These cofactors are also very simple to evaluate:

$$D(ZO, v'_1) = \left(\prod_{j \neq a_u} d'_j \right) e'_u \left(\prod_k d''_k \right), \quad (7)$$

$$D(ZO, a_u) = \left(\prod_{j \neq a_u} d'_j \right) \left(f - \sum_i \frac{c'_i e'_i}{d'_i} \right) \left(\prod_k d''_k \right) \quad (8a)$$

$$= \left[f \left(\prod_{j \neq a_u} d'_j \right) - \sum_i \left(\prod_{k \neq i, a_u} d'_k \right) c'_i e'_i \right] \left(\prod_k d''_k \right), \quad (8b)$$

$$D(ZO, a'_i) = \left(\prod_{j \neq a_u, a'_i} d'_j \right) (c'_i e'_u) \left(\prod_k d''_k \right). \quad (9)$$

As we noted above, FOCI wave functions are also invariant to unitary transformations among the virtual orbitals; however, there seems little to be gained by transforming the virtual orbitals to the corresponding orbital basis since the overlap between the virtual orbitals only enters Eq. (8) in a straightforward manner. It is also important to note that these formulas apply to the case where there are one or more rows and columns of zero in the valence-valence portion of the overlap matrix. This would occur if one or more of the d'_i 's were zero or if there was an orbital noncoincidence in the valence space.

$$\begin{array}{c}
 b'_1 \\
 b'_2 \\
 b'_3 \\
 b''_1 \\
 b''_2 \\
 b''_3 \\
 b'''_1 \\
 b'''_2 \\
 b'''_3
 \end{array}
 \left(
 \begin{array}{cccc|cc|cc|c}
 a'_1 & a'_2 & a'_3 & a'_4 & a''_1 & a''_2 & a'''_1 & a'''_2 & v'''_1 \\
 d'_1 & 0 & 0 & 0 & & & & & \\
 0 & d'_2 & 0 & 0 & & 0 & & & 0 \\
 0 & 0 & d'_3 & 0 & & & & & \\
 \hline
 & & & & d''_1 & 0 & & & \\
 & & & & 0 & d''_2 & & & 0 \\
 & & & & 0 & 0 & & & \\
 \hline
 & & & & & & d'''_1 & 0 & c'''_1 \\
 & & & & & & 0 & d'''_2 & c'''_2 \\
 & & & & & & 0 & 0 & c'''_3
 \end{array}
 \right)
 = S \quad .$$

\uparrow
 ZO_1

-ZO₂

-b_u

The only nonzero cofactor is

$$D(ZO_2, ZO_1) = \left(\prod_j d'_j \right) \left(\prod_k d''_k \right) c'''_u \left(\prod_l d'''_l \right). \quad (14)$$

Case III

Two configurations interact with virtual orbitals in different symmetries:

$$\begin{array}{c}
 b'_1 \\
 b'_2 \\
 b'_3 \\
 b''_1 \\
 b''_2 \\
 w''_1
 \end{array}
 \left(
 \begin{array}{cccc|cc}
 a'_1 & a'_2 & a'_3 & v'_1 & a''_1 & a''_2 \\
 d'_1 & 0 & 0 & c'_1 & 0 & 0 \\
 0 & d'_2 & 0 & c'_2 & 0 & 0 \\
 0 & 0 & d'_3 & c'_3 & 0 & 0 \\
 \hline
 0 & 0 & 0 & 0 & d''_1 & 0 \\
 0 & 0 & 0 & 0 & 0 & d''_2 \\
 0 & 0 & 0 & 0 & c''_1 & c''_2
 \end{array}
 \right)
 = S \quad .$$

The nonzero cofactors of the overlap matrix involve rows 3-6 and columns 1-4:

$$D(w''_1, v'_1) = \left(\prod_j d'_j \right) \left(\prod_k d''_k \right), \quad (10)$$

$$D(w''_1, a'_i) = \frac{c'_i}{d'_i} \left(\prod_j d'_j \right) \left(\prod_k d''_k \right) \quad (11a)$$

$$= c'_i \left(\prod_{j \neq i} d'_j \right) \left(\prod_k d''_k \right), \quad (11b)$$

$$D(b''_1, v'_1) = \left(\prod_j d'_j \right) \frac{c''_1}{d''_1} \left(\prod_k d''_k \right) \quad (12a)$$

$$= \left(\prod_j d'_j \right) c''_1 \left(\prod_{k \neq 1} d''_k \right), \quad (12b)$$

$$D(b''_1, a'_i) = \frac{c'_i}{d'_i} \left(\prod_j d'_j \right) \frac{c''_1}{d''_1} \left(\prod_k d''_k \right) \quad (13a)$$

$$= c'_i \left(\prod_{j \neq i} d'_j \right) c''_1 \left(\prod_{k \neq 1} d''_k \right). \quad (13b)$$

Case IV

One of the interacting configurations contains a virtual orbital in a passive symmetry while the other configuration contains only valence orbitals:

Case V

Both configurations contain virtual orbitals in the same passive symmetry:

$$\begin{array}{c}
 \begin{array}{cccc|cc|cc}
 a'_1 & a'_2 & a'_3 & a'_4 & a''_1 & a''_2 & a'''_1 & a'''_2 & v''' \\
 b'_1 & d'_1 & 0 & 0 & 0 & & & & \\
 b'_2 & 0 & d'_2 & 0 & 0 & & & 0 & \\
 b'_3 & 0 & 0 & d'_3 & 0 & & & & \\
 \hline
 b''_1 & & & & d''_1 & 0 & & & \\
 b''_2 & & 0 & & 0 & d''_2 & & & 0 \\
 b''_3 & & & & 0 & 0 & & & \\
 \hline
 b'''_1 & & & & & & d'''_1 & 0 & c_1 \\
 b'''_2 & & 0 & & & & 0 & d'''_2 & c_2 \\
 w''' & & & & & & e_1 & e_2 & f
 \end{array}
 \end{array}
 \quad -ZO_2$$

\uparrow
 ZO_1

The only nonzero cofactor is

$$D(ZO_2, ZO_1) = \left(\prod_i d'_i \right) \left(\prod_j d''_j \right) \left(\prod_k d'''_k \right) \left(f - \sum_k \frac{e_k c_k}{d'''_k} \right). \quad (15)$$

Case VI

Both configurations contain virtual orbitals but only one of the virtual orbitals is in an active symmetry:

$$\begin{array}{c}
 \begin{array}{cccc|cc|ccc}
 a'_1 & a'_2 & a'_3 & v' & a''_1 & a''_2 & a'''_1 & a'''_2 & a'''_3 \\
 b'_1 & d'_1 & 0 & 0 & c_1 & & & & \\
 b'_2 & 0 & d'_2 & 0 & c_2 & 0 & & & 0 \\
 b'_3 & 0 & 0 & d'_3 & c_3 & & & & \\
 \hline
 b''_1 & & & & & d''_1 & 0 & & \\
 b''_2 & & 0 & & & 0 & d''_2 & & 0 \\
 b''_3 & & & & & 0 & 0 & & \\
 \hline
 b'''_1 & & & & & & & d'''_1 & 0 & 0 \\
 b'''_2 & & 0 & & & & & 0 & d'''_2 & 0 \\
 w''' & & & & & & & e_1 & e_2 & e_3
 \end{array}
 \end{array}
 \quad -ZO$$

\uparrow
 a_u

This case is actually a generalization of case I with the last term in Eq. (5) being replaced by

$$\left(e_{a_u} \prod_k d'''_k \right). \quad (16)$$

It is also important to note that the cofactor $D(ZO, a_u)$ is zero in this case.

SECOND-ORDER CI

Most of the formulas which are needed to obtain the transition moments when second-order CI wave functions are employed can also be generated in a straightforward fashion. Many of the cases encountered in a second-order calculation can be treated as a product of one or more of the cases encountered in the discussion of a first-order calculation. In a few cases the overlap matrix that arises in a second-order calculation is sufficiently complex that the cofactors must be evaluated with the biorthogonalization scheme of Prosser and Hagstrom.¹⁵ However, even in these cases the utilization of corresponding orbitals still offers the advantage of rapid detection of zeros. One such case is discussed below.

In this case all virtual orbitals are in the same active symmetry:

TABLE III. Full valence MCSCF and CI results for OF.^a

	² Δ orbitals	² Π orbitals
² Δ	-174.004 317	-173.953 750
² Π	-174.246 015	-174.257 807
ΔE	0.241 698	0.304 057
Orthogonal TM	0.029 800	0.051 000
Optimum ΔE = 0.25349 nonorthogonal optimum TM = 0.0334		

^aAll quantities are in atomic units.

and the 1σ orbitals were frozen in all calculations. These orbitals were obtained from *b*-state (⁴Σ_g⁻) SCF calculations. In Table I we compare our results to those obtained by Tanaka and Yoshimine²¹ in which they employed a basis of Slater orbitals. In Table II, the overlaps between the corresponding orbitals obtained in the three calculations are presented.

The nonorthogonal and orthogonal transition moments are in close agreement with the results of Tanaka and Yoshimine. At this level of approximation, the *c*-state (⁴Σ_g⁻) orbitals offer a very good representation of the three states investigated. The very high overlaps between the sets of corresponding orbitals show that the valence space is very similar for all states, so it is not surprising that orthogonal orbitals work well in this case.

OF

Full valence MCSCF (including the 2s orbitals) calculations were performed on the ²Π and ²Δ states of OF. van Duijneveldt's 11s6p Gaussian basis was used and contracted as before. This basis was also augmented by two *d* functions on each center with exponents 2.901, 0.6194, 2.214, and 0.655 on oxygen and fluorine. The results of the OF calculations are presented in Table III and the overlaps of the corresponding orbitals are presented in Table IV. These calculations were carried out in C_{2v} symmetry which led to CI expansions of 42 and 18 CSF's for the ²Δ and the ²Π states, respectively. All of the transition moment calculations (which were undertaken in the corresponding orbital basis) required approximately an order of magnitude less time than the equivalent general nonorthogonal transition moment calculation.

In the OF calculations, the Prosser-Hagstrom non-orthogonal transition moment calculation required 25 cp sec while the equivalent corresponding orbital calculation required 2 cp sec. The orthogonal transition moment calculation required approximately 2 cp sec as well. (These calculations were performed on a CDC Cyber 173 computer.)

A nonorthogonal treatment of OF clearly indicated that the transition moment and the energy separation fluctuate significantly when different sets of orthogonal orbitals are used in the calculation. The excited state orbitals clearly provide a better description of both states than do the ground state orbitals. The overlap

TABLE IV. Corresponding orbital overlaps for OF.

	3σ	4σ	5σ	6σ	1π	2π
(² Π ⁺ Δ)	0.999 998	0.999 990	0.999 789	0.975 120	0.999 986	0.999 703

between the corresponding orbital reflects significant orbital reorganization in the excited state. Therefore, it is not surprising to find that the TM obtained in orthogonal and nonorthogonal calculations do not coincide. This case is more representative than O₂⁺ where the orbitals are virtually the same for both states. This effect is expected to become even more pronounced in heteronuclear diatomics which possess a large ionic character.^{2,3}

CONCLUSIONS

Corresponding orbitals provide a very convenient basis in which to calculate transition moments from full valence and first-order CI wave functions. Moreover, corresponding orbitals have been shown to reduce the work needed to compute the cofactors of the overlap matrices and to detect zero contributions to the transition density matrix. In the case of the first-order CI, the higher the symmetry, the more efficient is the zero detection.

This technique provides an attractive compromise between the standard orthogonal transition moment algorithm and the nonorthogonal transition moment method of Prosser and Hagstrom.¹⁵ This is especially true in large CI calculations in which the states of interest are poorly described by the same orbital basis.

It is also noted that the overlap between the corresponding orbitals can be used to identify the systems in which a nonorthogonal calculation is required.

¹H. F. Schaefer III, *The Electronic Structure of Atoms and Molecules: A Survey of Rigorous Quantum Mechanical Results* (Addison-Wesley, Reading, Mass., 1972).

²C. W. Bauschlicher, Jr., B. H. Lengsfeld, III, and D. R. Yarkony, *J. Chem. Phys.* **73**, 5702 (1980).

³C. W. Bauschlicher, B. H. Lengsfeld, III, D. M. Silver, and D. R. Yarkony, *J. Chem. Phys.* **74**, 2379 (1981).

⁴H. F. Schaefer III, in *Energy, Structure, and Reactivity: Proceedings of the 1972 Boulder Conference*, edited by D. R. Smith and W. B. Merae (Wiley, New York, 1973).

⁵M. Yoshimine, A. D. McLean, and B. Liu, *J. Chem. Phys.* **58**, 4412 (1973).

⁶F. Weinhold, *J. Chem. Phys.* **54**, 1874 (1971).

⁷S. R. Langhoff and D. P. Chong, *J. Chem. Phys.* **69**, 1974 (1978).

⁸A. T. Amos and G. G. Hall, *Proc. R. Soc. London Ser. A* **263**, 483 (1961).

⁹P. E. M. Siegbahn, J. Almlöf, A. Heiberg, and B. Roos, *J. Chem. Phys.* **74**, 2384 (1981).

¹⁰B. Roos, P. R. Taylor, and P. E. M. Siegbahn, *Chem. Phys.* **48**, 157 (1980).

¹¹J. E. Harriman, *J. Chem. Phys.* **40**, 2827 (1964); K. M. Sando and J. E. Harriman, *ibid.* **47**, 180 (1967).

¹²R. L. Martin and E. R. Davidson, *Phys. Rev. A* **16**, 1341 (1977).

¹³P. Bagus (private communication).

¹⁴H. F. King, R. E. Stanton, H. Kiu, R. E. Wayatt, and R. G.

- Parr, *J. Chem. Phys.* **47**, 1936 (1967).
- ¹⁵F. Prosser and S. Hagstrom, *Int. J. Quantum Chem.* **2**, 89 (1968).
- ¹⁶E. R. Davidson, *Reduced Density Matrices in Quantum Chemistry* (Academic, New York, 1976).
- ¹⁷B. H. Lengsfield, III and J. C. Schug, *Mol. Phys.* **35**, 1113 (1978).
- ¹⁸H. F. Schaefer III, R. H. Klemm, and F. E. Harris, *Phys. Rev.* **181**, 137 (1969).
- ¹⁹MOLECULE is a Gaussian integral program written by J. Almlöf of the University of Uppsala, Sweden. For a description of MOLECULE see J. Almlöf, in *Proceedings of the Second Seminar on Computational Problems in Quantum Chemistry* (Max-Planck-Institut, Munich, 1973), p. 14. NONAME is a general SCF-MCSCF open-ended CI program written by C. W. Bauschlicher, Jr. and B. H. Lengsfield, III.
- ²⁰F. B. van Duijneveldt, "Gaussian Basis Sets for the Atoms H-Ne for Use in Molecular Calculations," Research Report RJ945, International Business Machines Corp., San Jose, Calif., 10 December, 1971.
- ²¹K. Tanaka and M. Yoshimine, *J. Chem. Phys.* **70**, 626 (1979).